HUNTING FOR WILD ANTARCTIC ASTRO-PARTICLES

J. C. Hanson (CCAPP, The Ohio State University)

April 11, 2017

Earth Sciences 5650, Glaciology

HUNTING FOR WILD ANTARCTIC ASTRO-PARTICLES

I. **UHE-ν** observations, and a 100-year physics problem
   A. UHE: Ultra-high energy $\approx$ 1 EeV (10^{18} eV), or 0.1 J
II. **Antarctica** is not a *venue*, but a *target*
   A. The Askaryan effect
   B. Ice properties
III. **Undergraduate research with ARA and ARIANNA**
   A. Idea $\rightarrow$ Design $\rightarrow$ Testing $\rightarrow$ Deploy $\rightarrow$ Analysis
   B. Monte Carlo simulations, glaciological modeling
   C. RF circuit/antenna design, systems integration
   D. Logistics
IV. The ARIANNA-HRA, and Recent Results
V. ARA2, and Recent Results
VI. **Future Opportunities**

UHE-ν OBSERVATIONS, AND A 100-YEAR PHYSICS PROBLEM

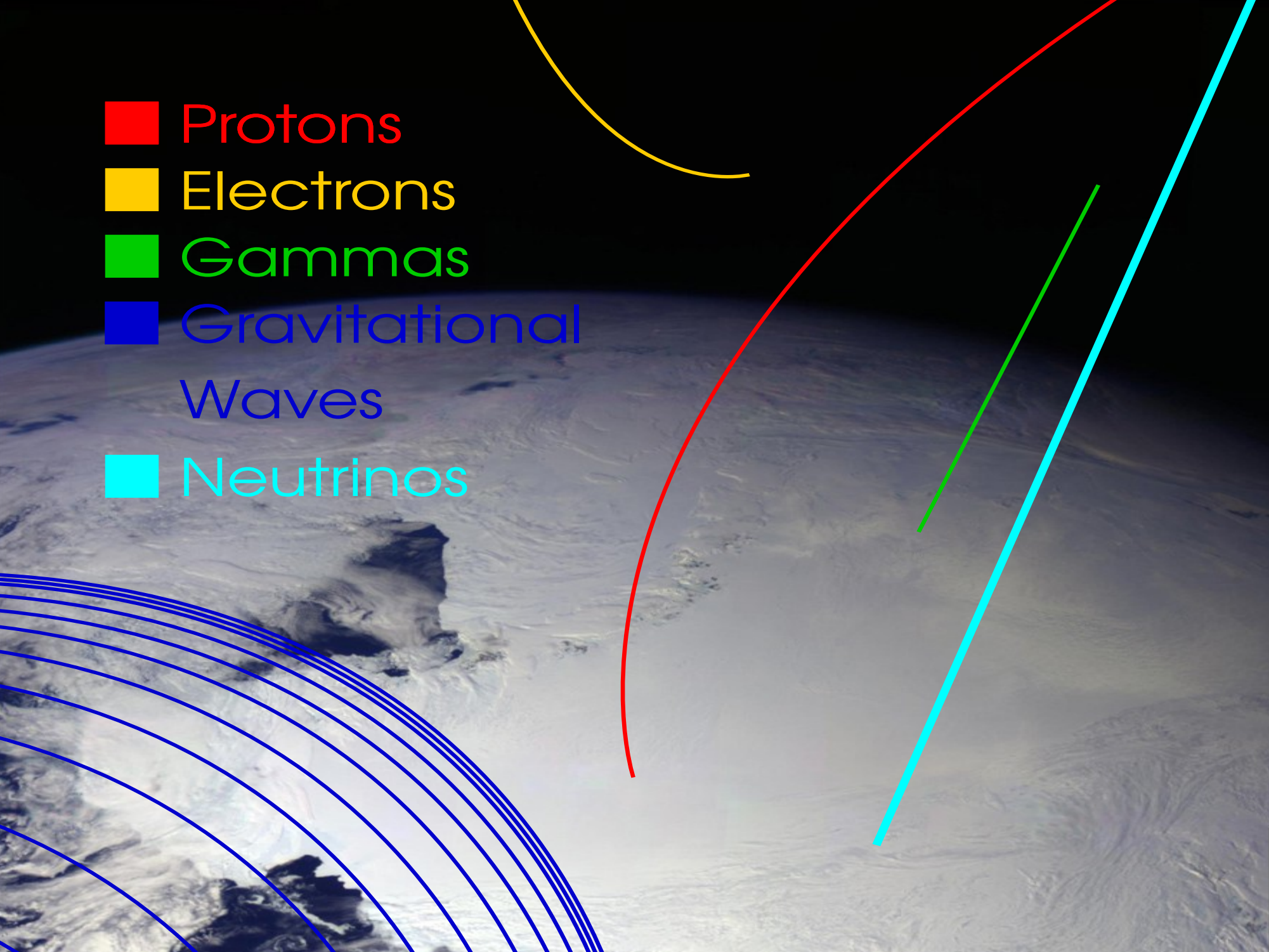
Protons
Electrons
Gammas
Gravitational Waves
Neutrinos

THE UHE COSMIC-RAYS (UHECR): PROTONS AND NUCLEI AT THE HIGHEST ENERGIES

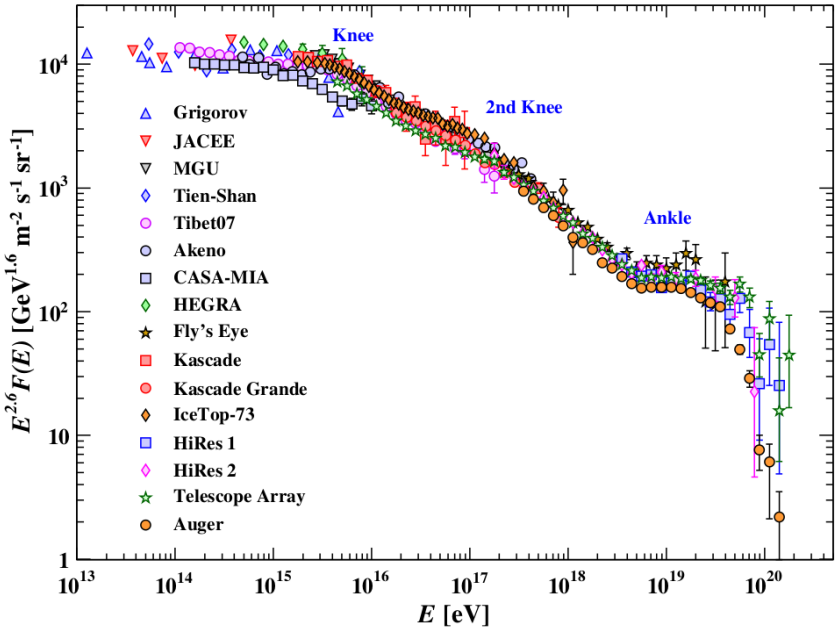

Figure 1: CR energy spectrum [9]

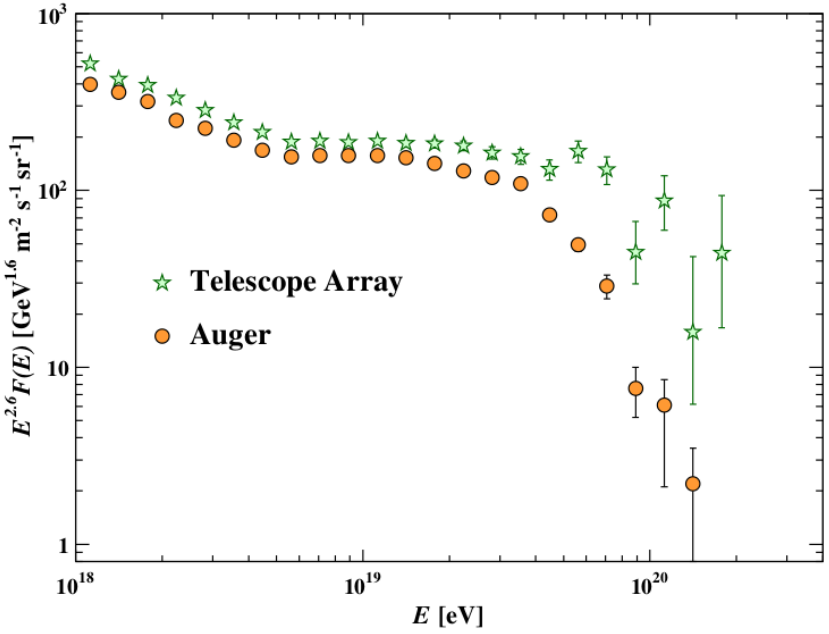

Figure 2: Figure 1, EeV scale [10]

Energies per nucleus span ***seven orders of magnitude***.

GZK PROCESS, UHECR $\rightarrow$ UHE-ν

The ***GZK Process*** describes UHE-ν production when CR's interact with the Cosmic Microwave Background (CMB):

$$\boxed{p^+ + \gamma_{CMB} \rightarrow n^0 + e^+ + \bar{\nu} + \nu + \nu} \tag{1}$$

$$\rightarrow \boxed{n^0 \rightarrow p^+ + e^- + \bar{\nu}} \tag{2}$$

$$\boxed{p^+ + \gamma_{CMB} \rightarrow p^+ + \gamma + \gamma} \tag{3}$$

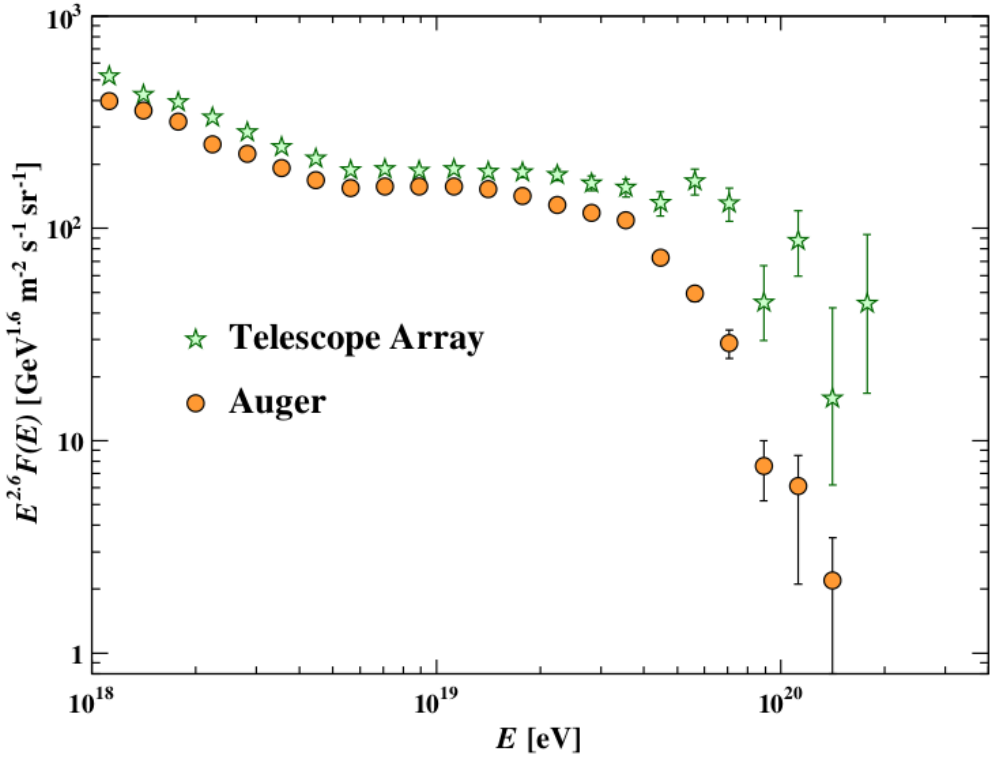

Figure 3: The drop in flux at right is most likely caused by the GZK effect [10].

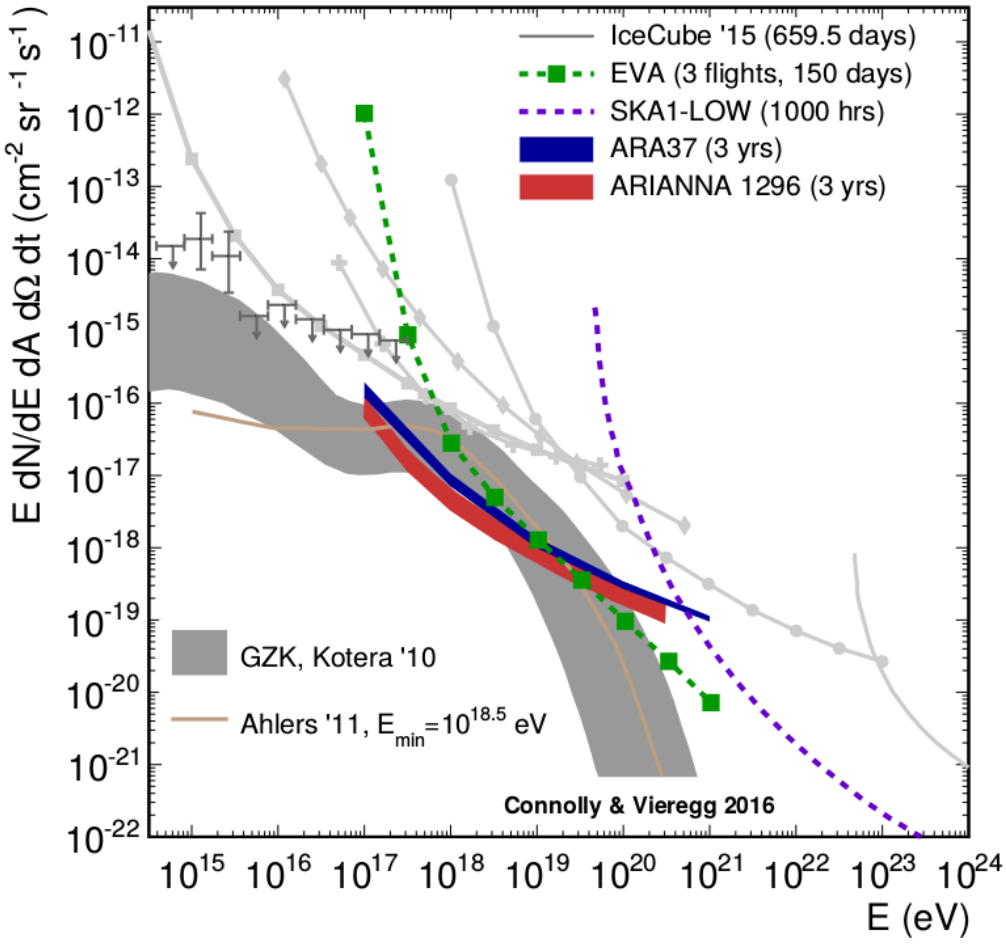

Figure 4: Predicted UHE-ν fluxes from UHECR flux at Earth [1].

ANTARCTICA IS NOT THE VENUE, BUT THE TARGET

WE NEED A BIG TARGET: EFFECTIVE VOLUME AND ICE PROPERTIES

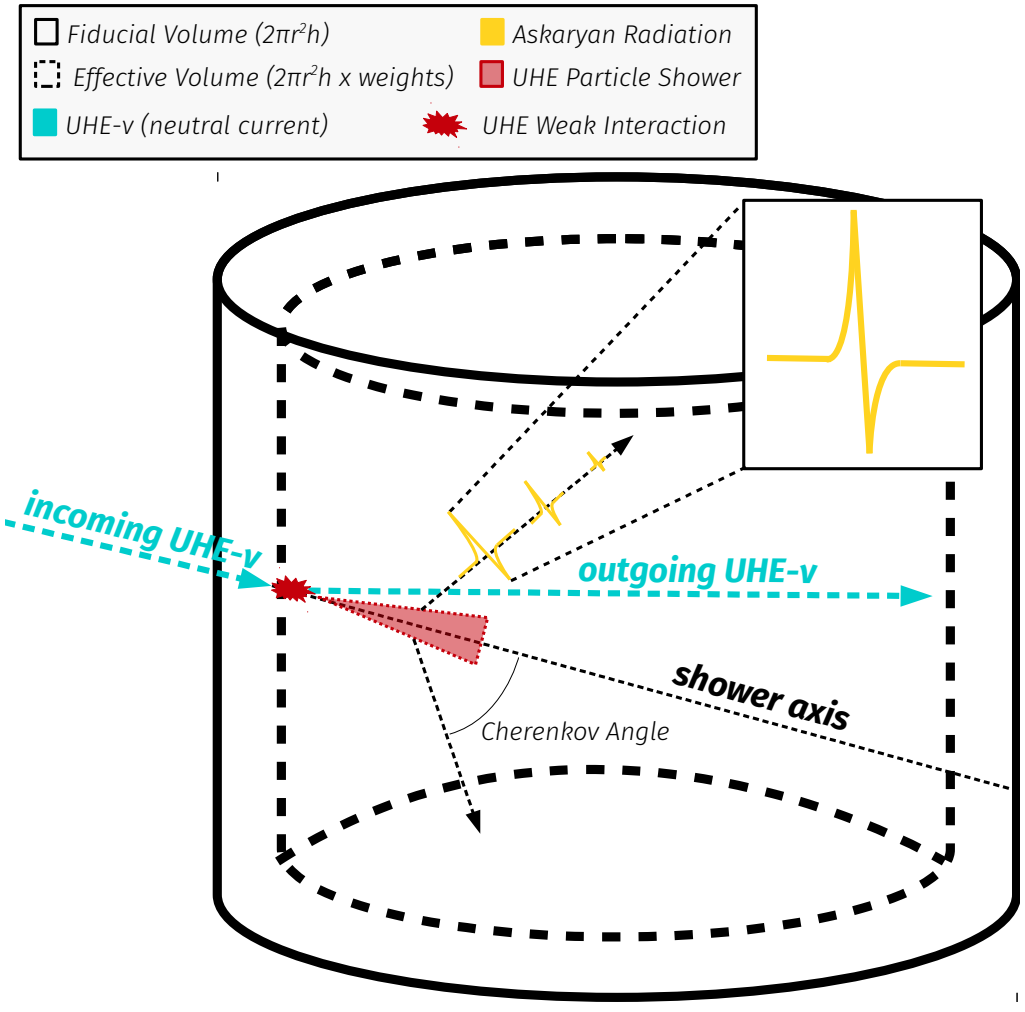

Figure 5: Concepts of effective volume, and attenuation length.

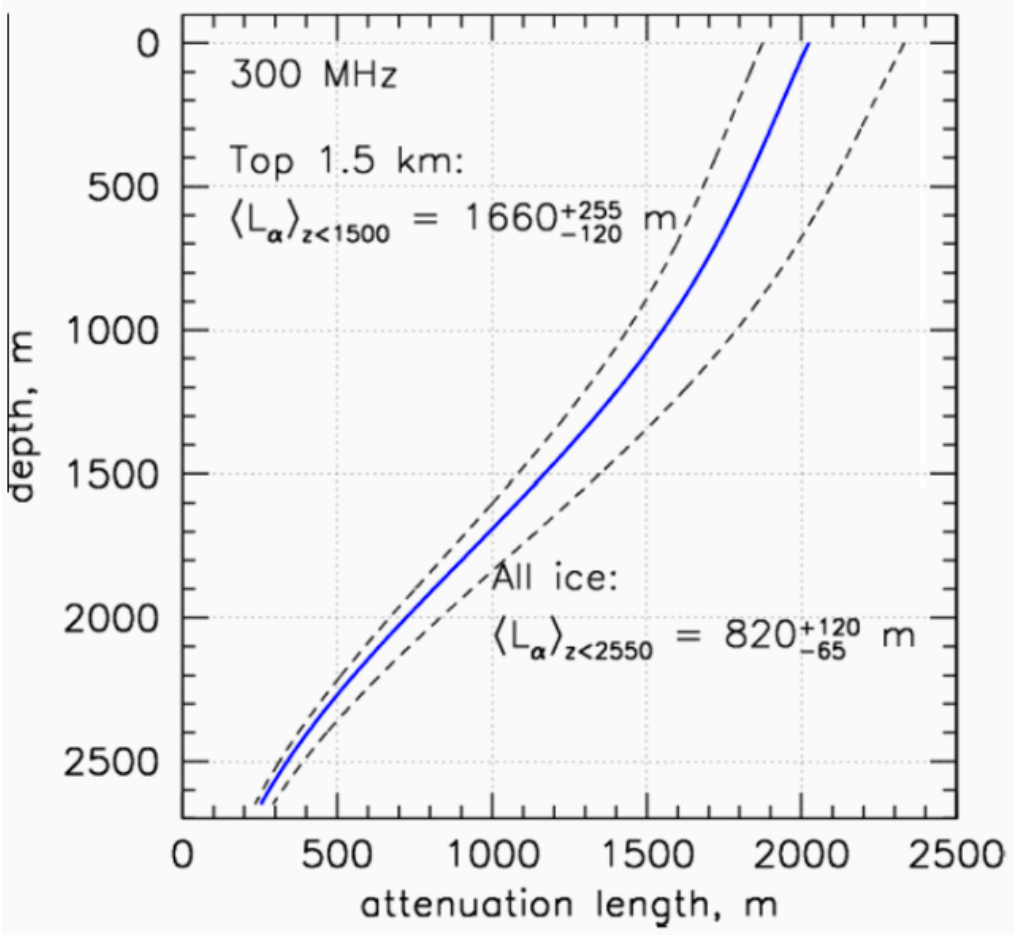

Figure 6: The attenuation length versus depth at the South Pole [3].

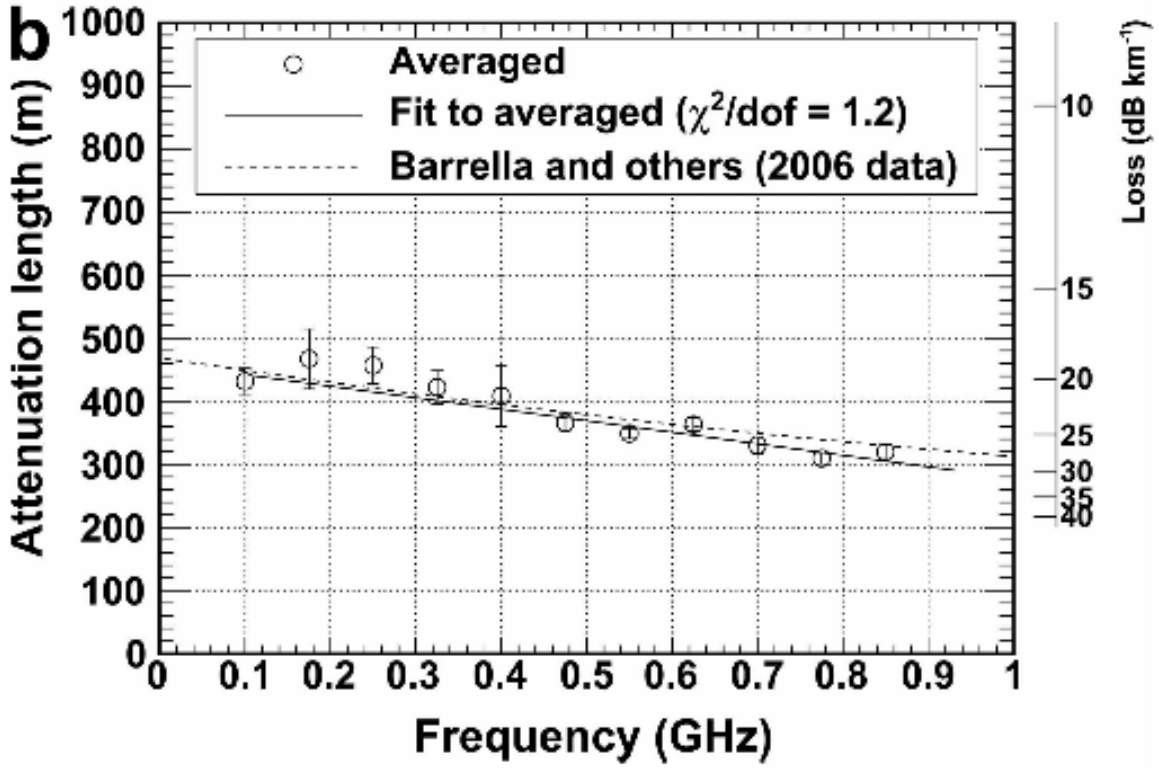

Figure 7: The attenuation length versus depth in Moore's Bay [5].

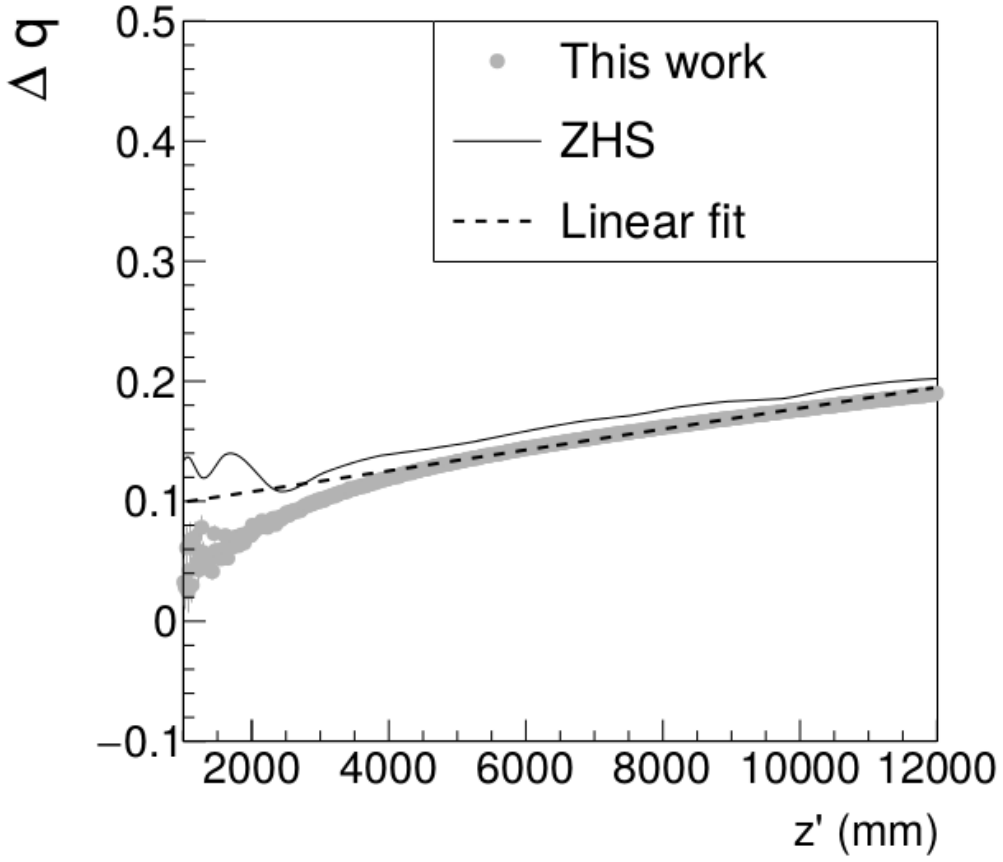

Figure 8: As the cascade progresses, the negative charge excess increases [8].

THE ASKARYAN EFFECT - FIRST OBSERVATION AT SLAC

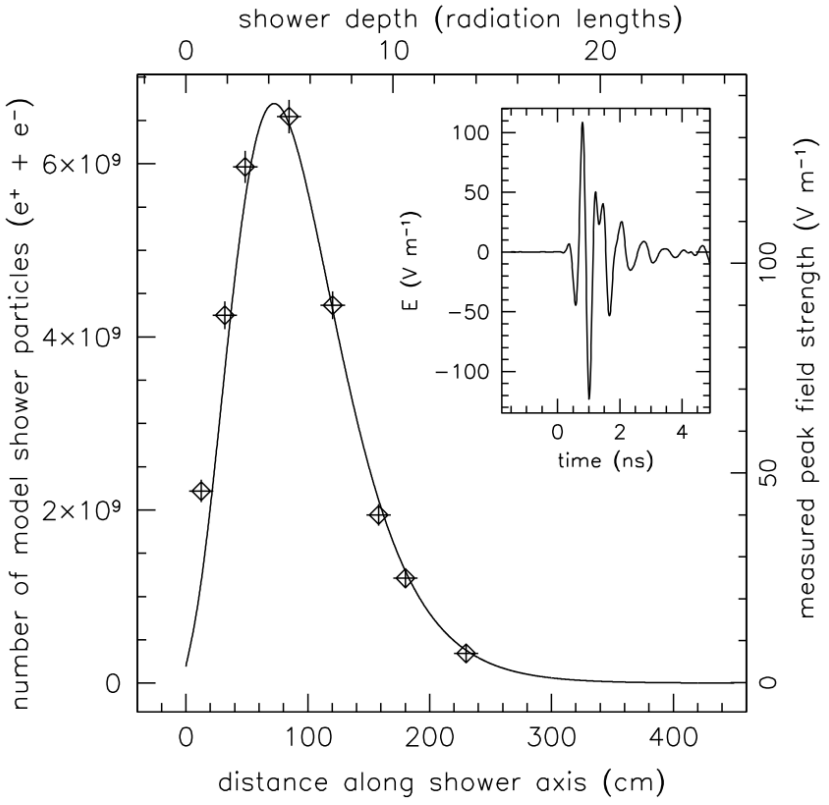

Figure 9: D. Saltzberg et al. observed the Askaryan Effect at SLAC [13].

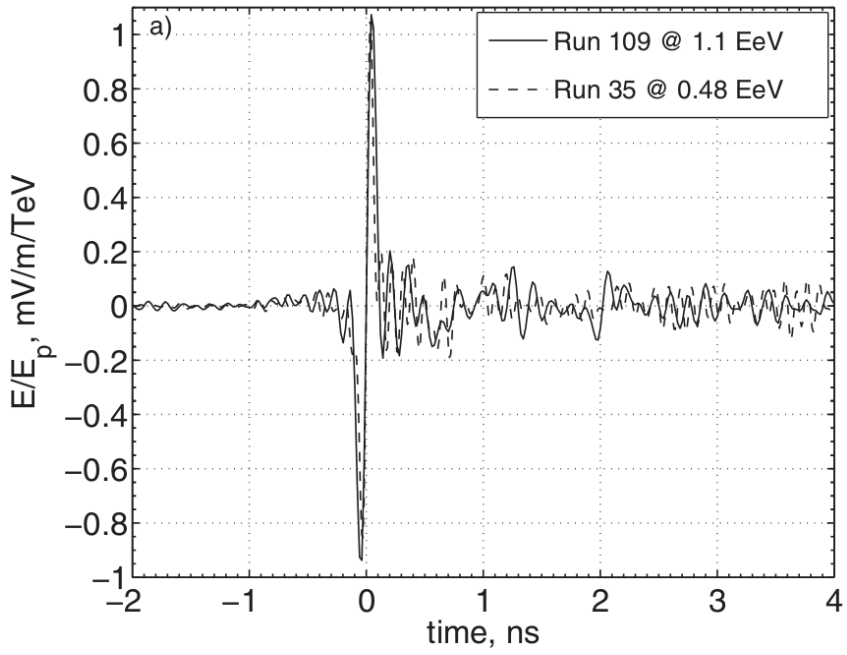

Figure 10: An example of an Askaryan radio-frequency (RF) impulse [11].

Figure 11: A second test at SLAC demonstrated the Askaryan effect in ice [7].

TWO EXPERIMENTS: ARA AND ARIANNA

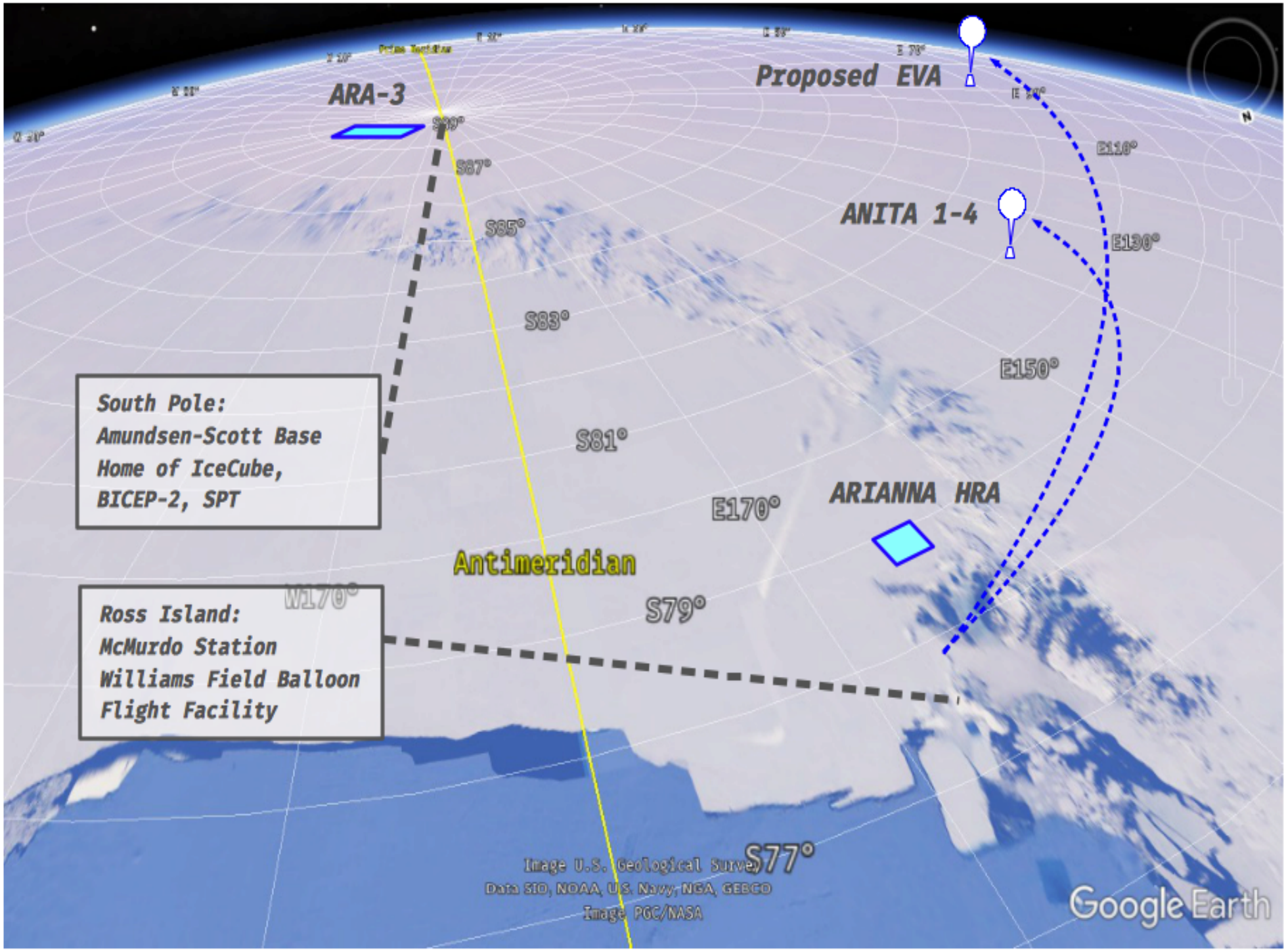
ARA-3
Proposed EVA
ANITA 1-4
ARIANNA HRA
Antimeridian
South Pole:
Amundsen-Scott Base
Home of IceCube,
BICEP-2, SPT
Ross Island:
McMurdo Station
Williams Field Balloon
Flight Facility
S89°
S87°
S85°
S83°
S81°
S79°
S77°
E110°
E130°
E150°
E170°
W170°
Image U.S. Geological Survey
Data SIO, NOAA, U.S. Navy, NGA, GEBCO
Image PGC/NASA
Google Earth

ANTARCTIC ROSS ICE SHELF ANTENNA NEUTRINO ARRAY (ARIANNA)

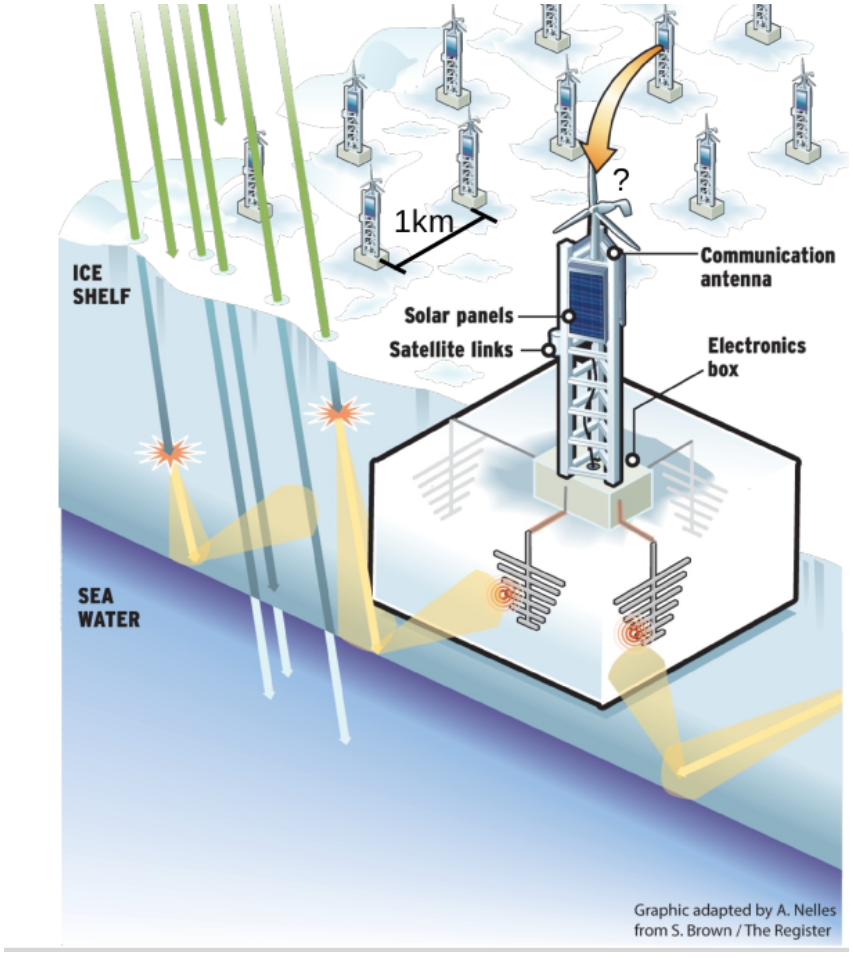

Figure 12: ARIANNA is deployed on the Ross Ice Shelf, using the ocean as a reflective surface for Askaryan RF pulses.

ASKARYAN RADIO ARRAY (ARA)

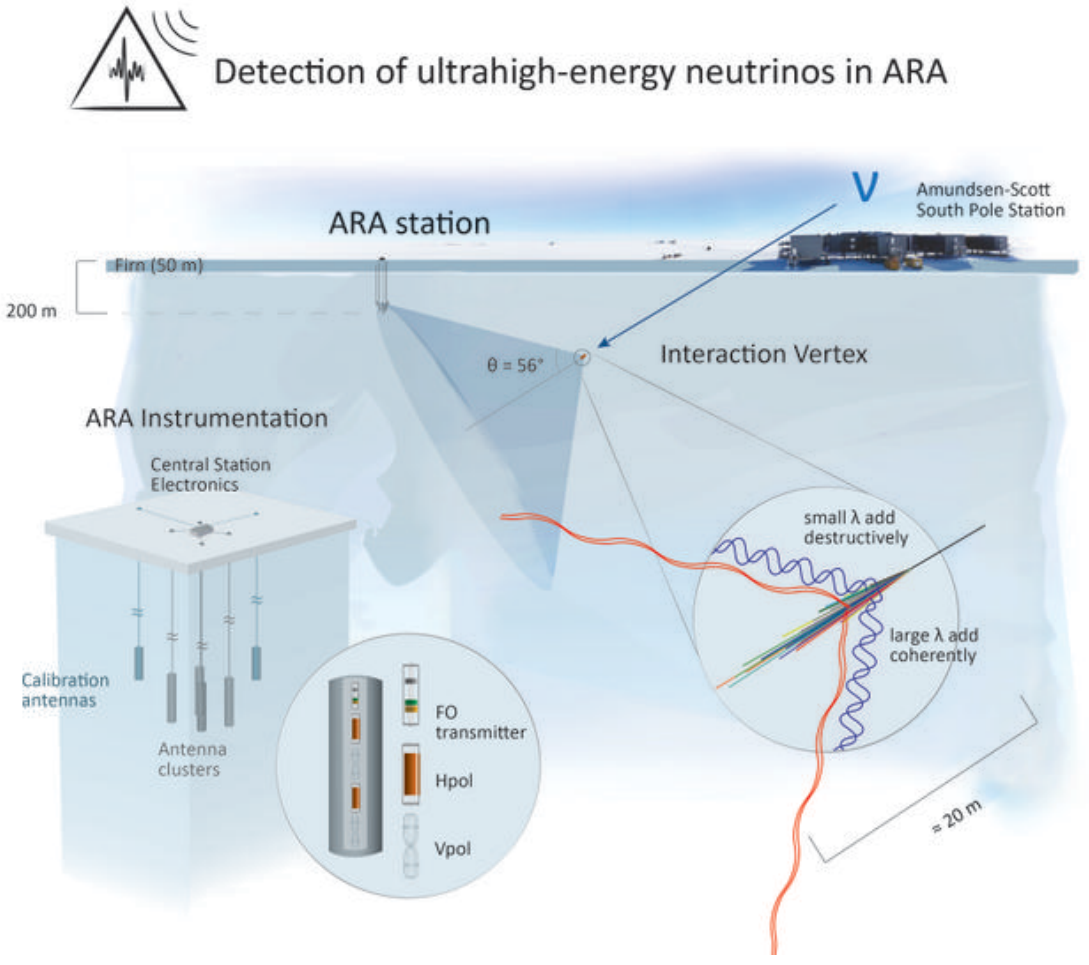

Figure 13: ARA is deployed at the South Pole, taking advantage of the clearest ice on the planet.

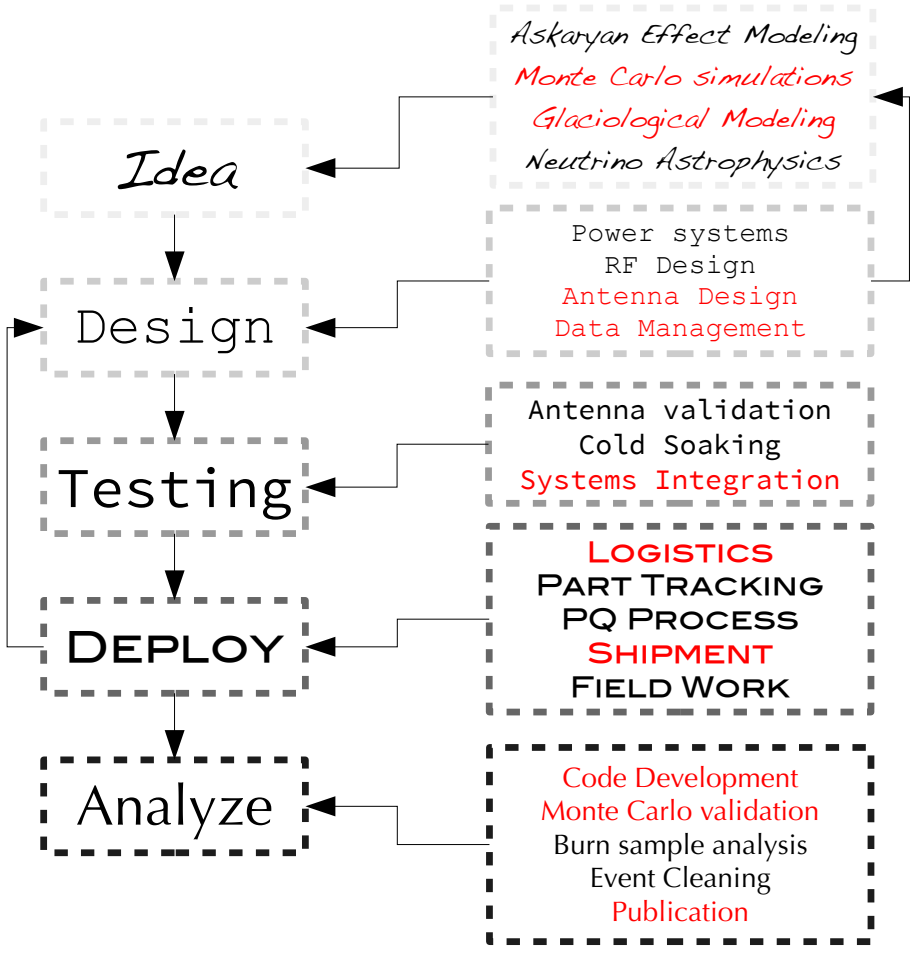

Figure 14: (Red) Contributions from undergraduates.

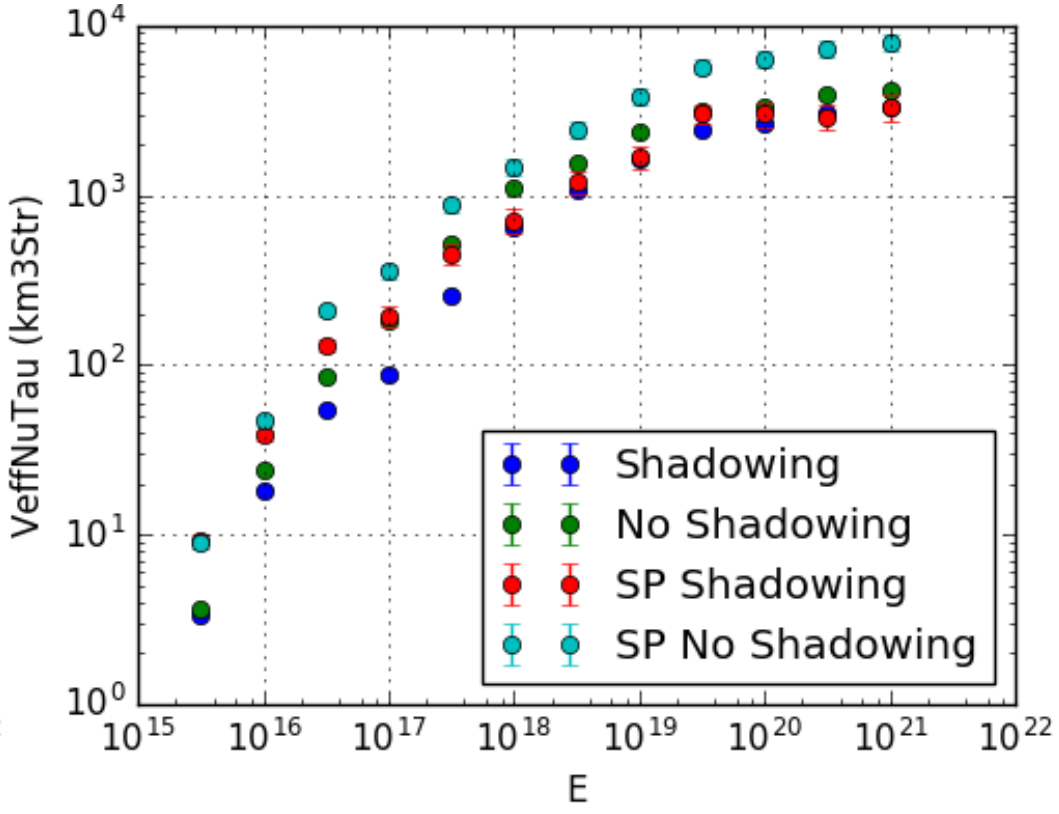

Figure 15: ARIANNA MC demonstrates the effect of Moore's Bay ice versus South Pole ice, and the *firn*. Courtesy of C. Persichilli (UC Irvine).

- Simulations produce $V_{eff}\Omega(E)$
- Activating various effects shows relative importance
- Example: South Pole vs. Moore's Bay, *firn*

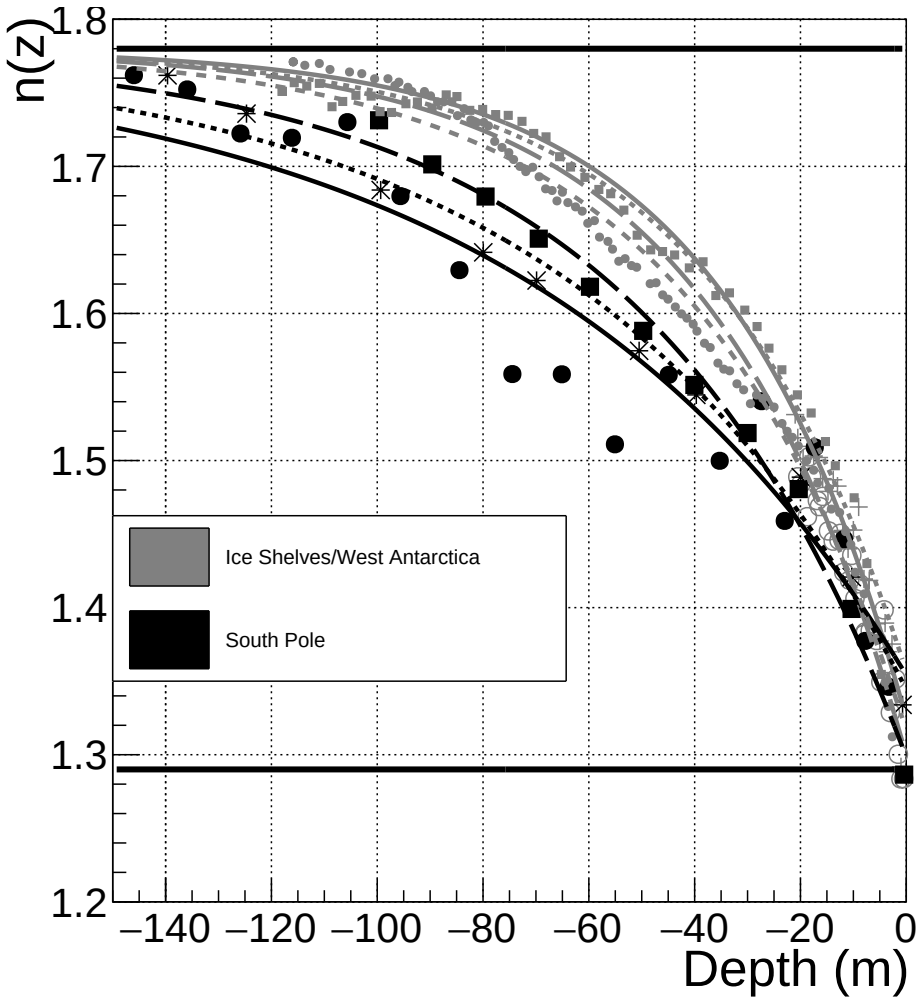

Figure 16: The index of refraction versus depth.

- Activating various effects shows relative importance
- The firn causes light rays to bend
- We require a solution to exist between cascade and station

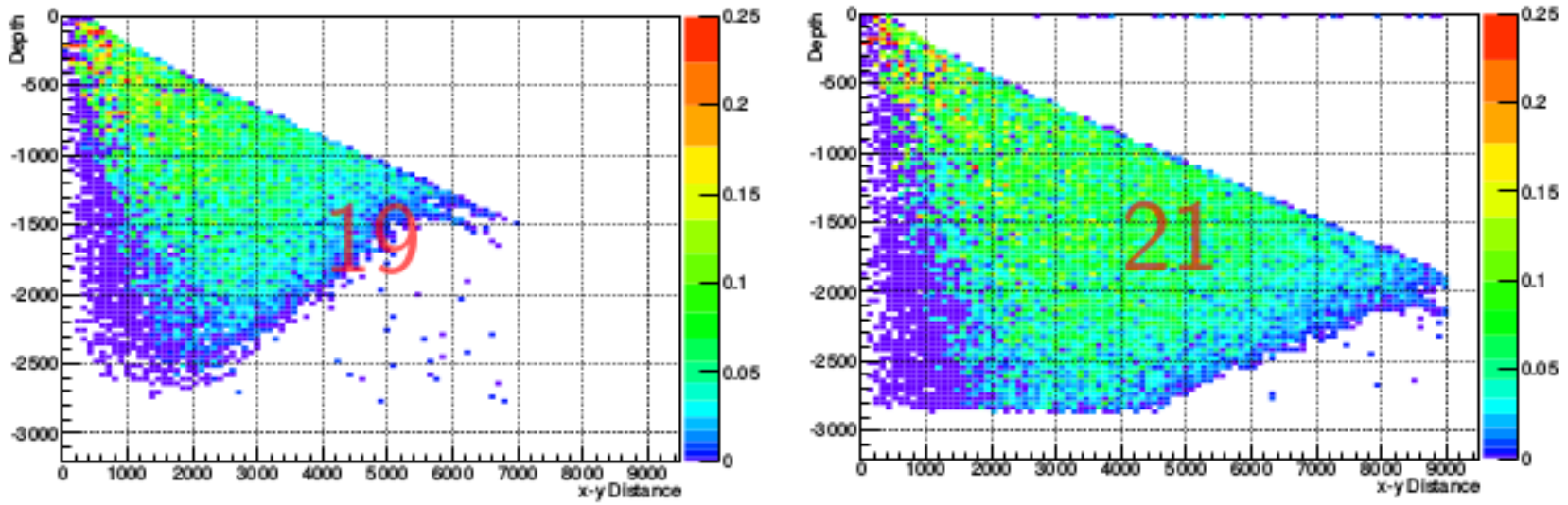

Figure 17: Glaciological evidence for shadowing being reviewed. Figure courtesy of Andrew Shultz, University of Nebraska (Physics).

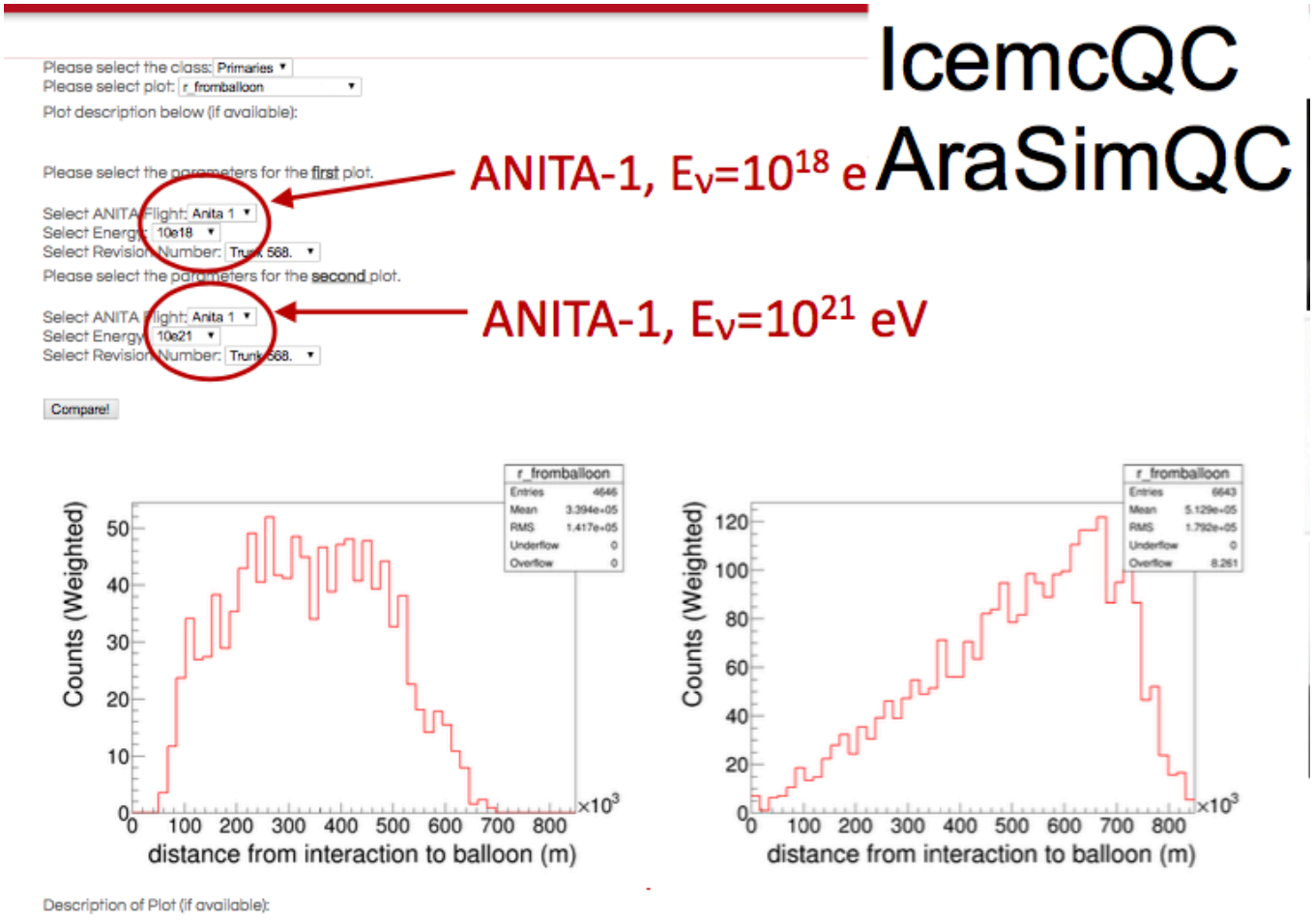

Figure 18: Undergraduates have helped us track online the physics modifications to the simulations: AraSimQC. Pictured: UHE-ν with different energies for the same detector.

Figure 19: (Top row, left to right) Kaeli Hughes, Jude Rajasekara, Hannah Hasan. (Bottom row, left to right) Jorge Espinosa, Chris Persichilli.

Figure 20: Computing in High-Energy Physics Research (CHEAPR) 2016. Workshop devoted to exploring how machine-learning can improve our Askaryan signal recognition **http://ccapp.osu.edu/workshops/CHEAPR2016/workshop.html**.

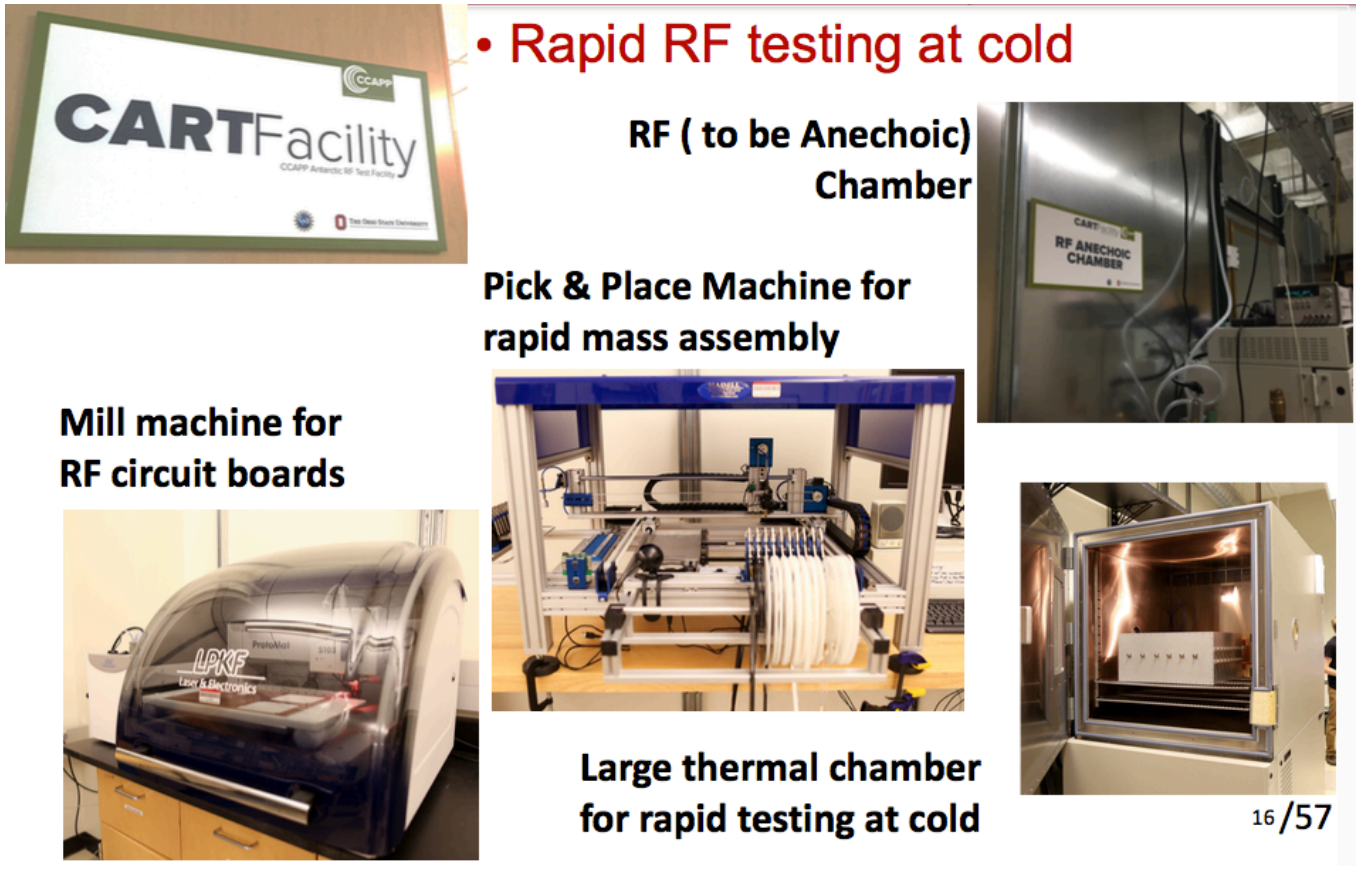

Figure 21: Undergraduates and graduate students are responsible for ARA systems integration at Ohio State.

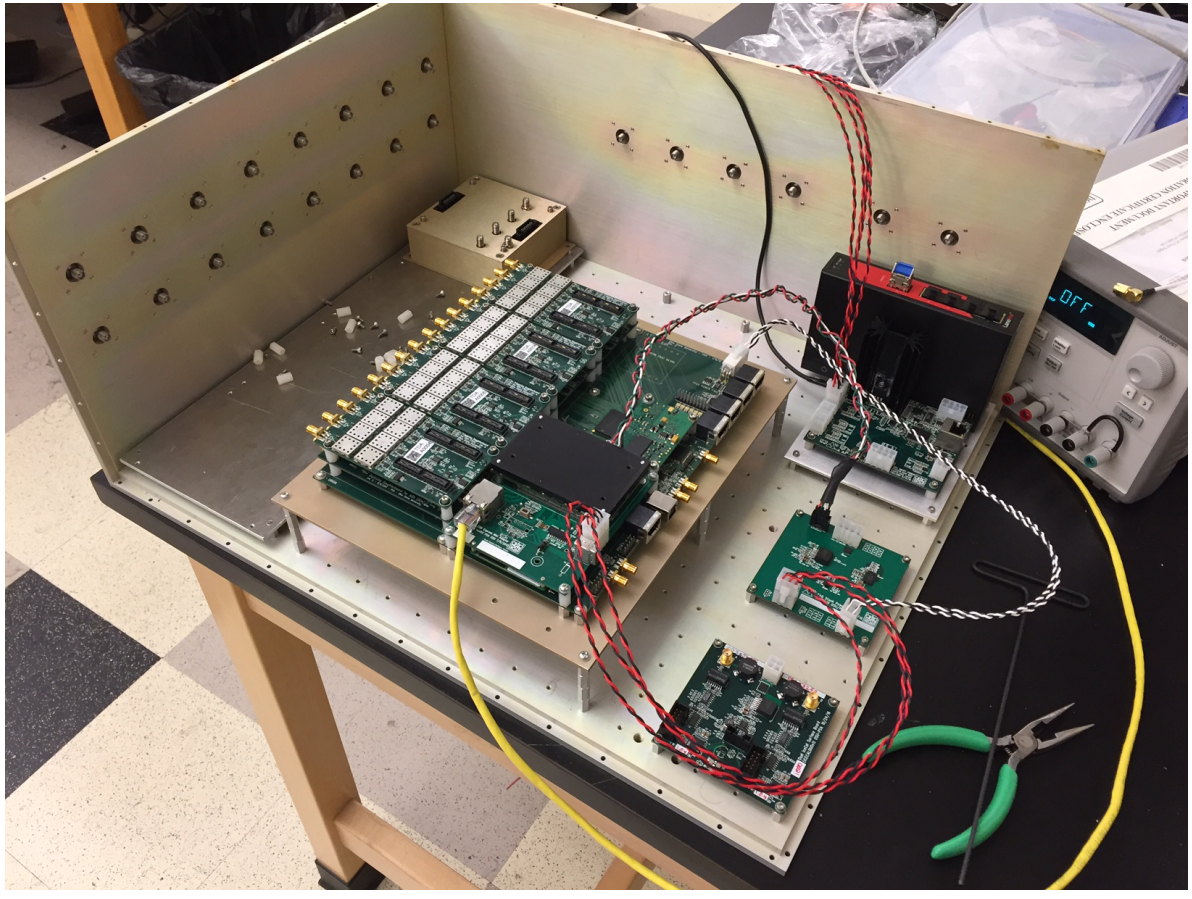

Figure 22: ARA-4 during systems integration.

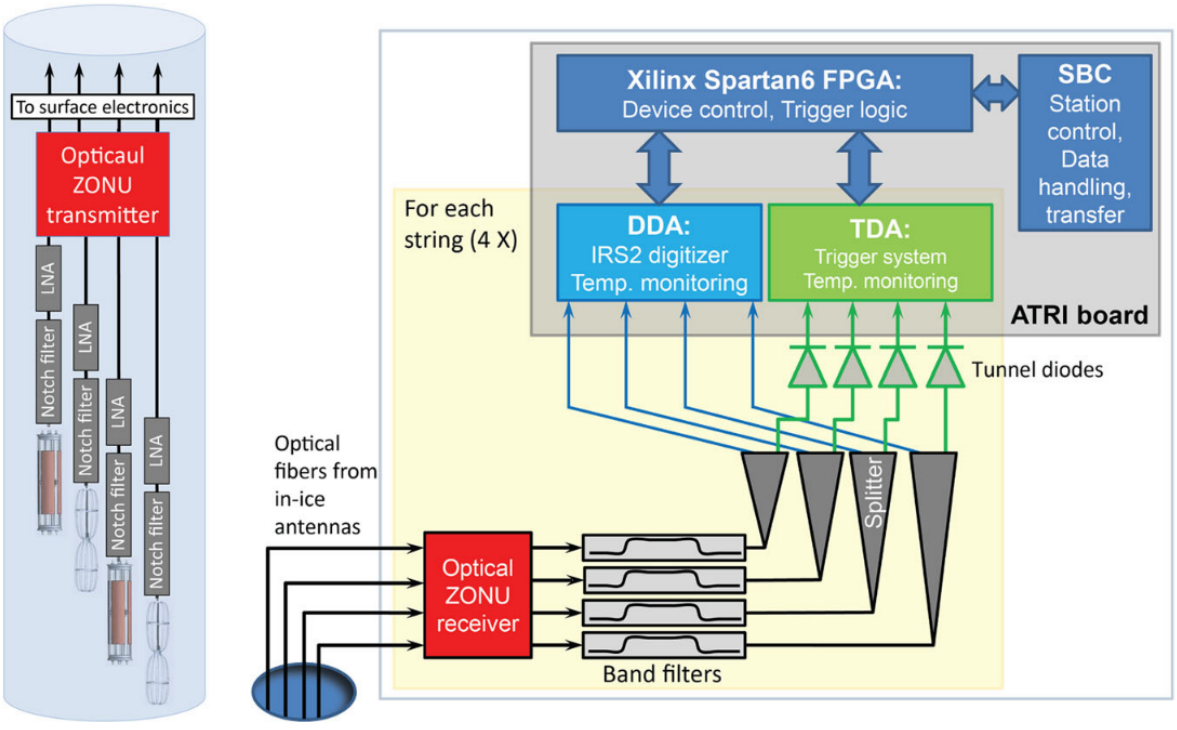

Figure 23: The general design of the ARA stations [2].

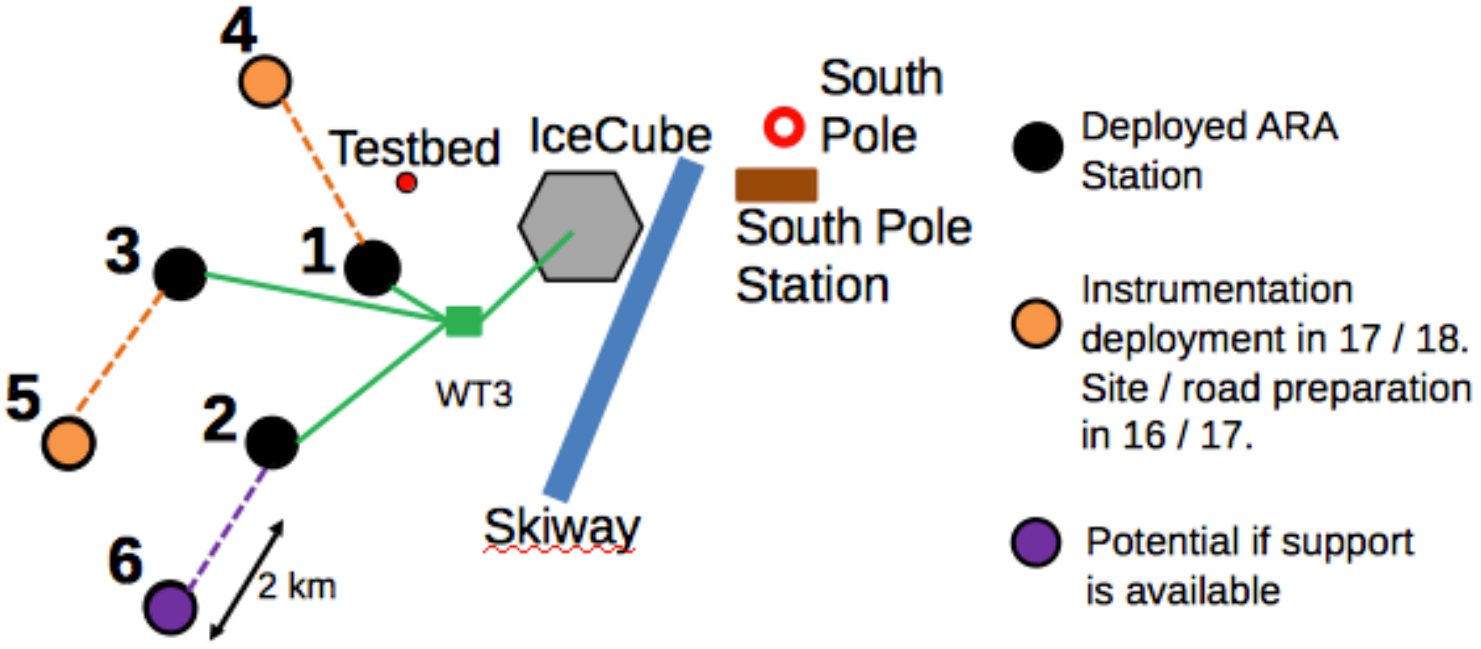

Figure 24: Planned ARA deployment for 2017 Antarctic season.

Figure 25: (Left to Right) Patrick Allison, Oindree Banerjee, Brian Clark

Not pictured: Mike Kovacevish, Lucas Smith, Suren Gourapura

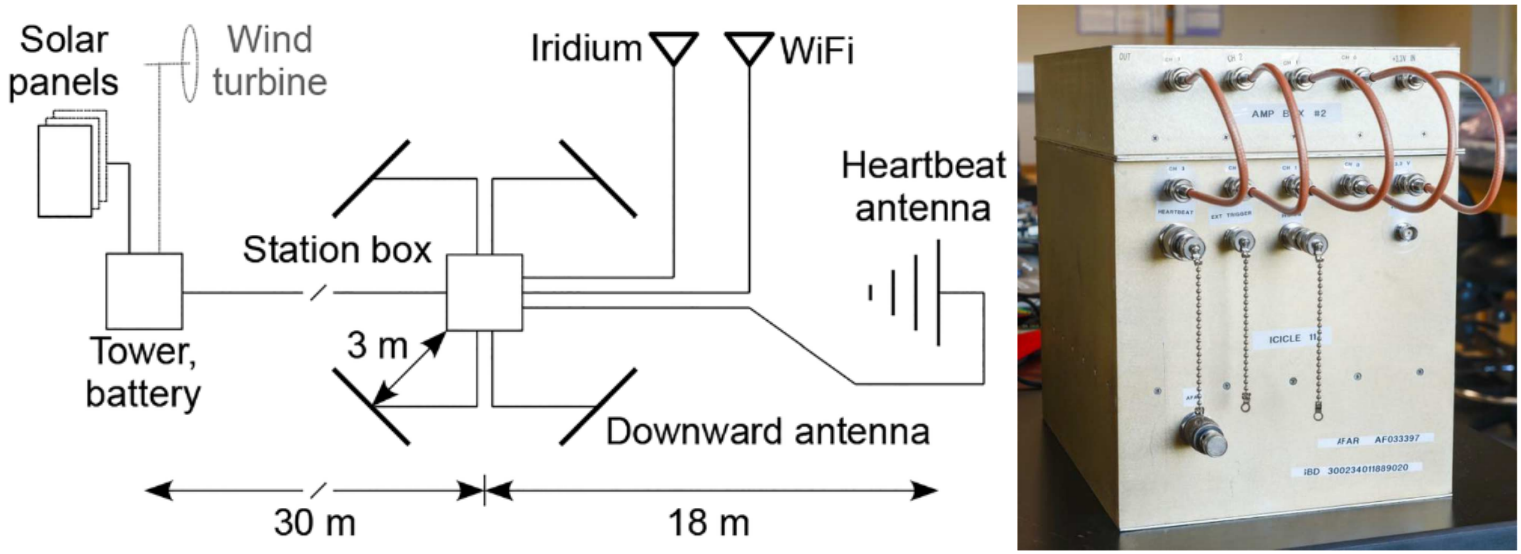

Figure 26: The general design of the ARIANNA systems [6].

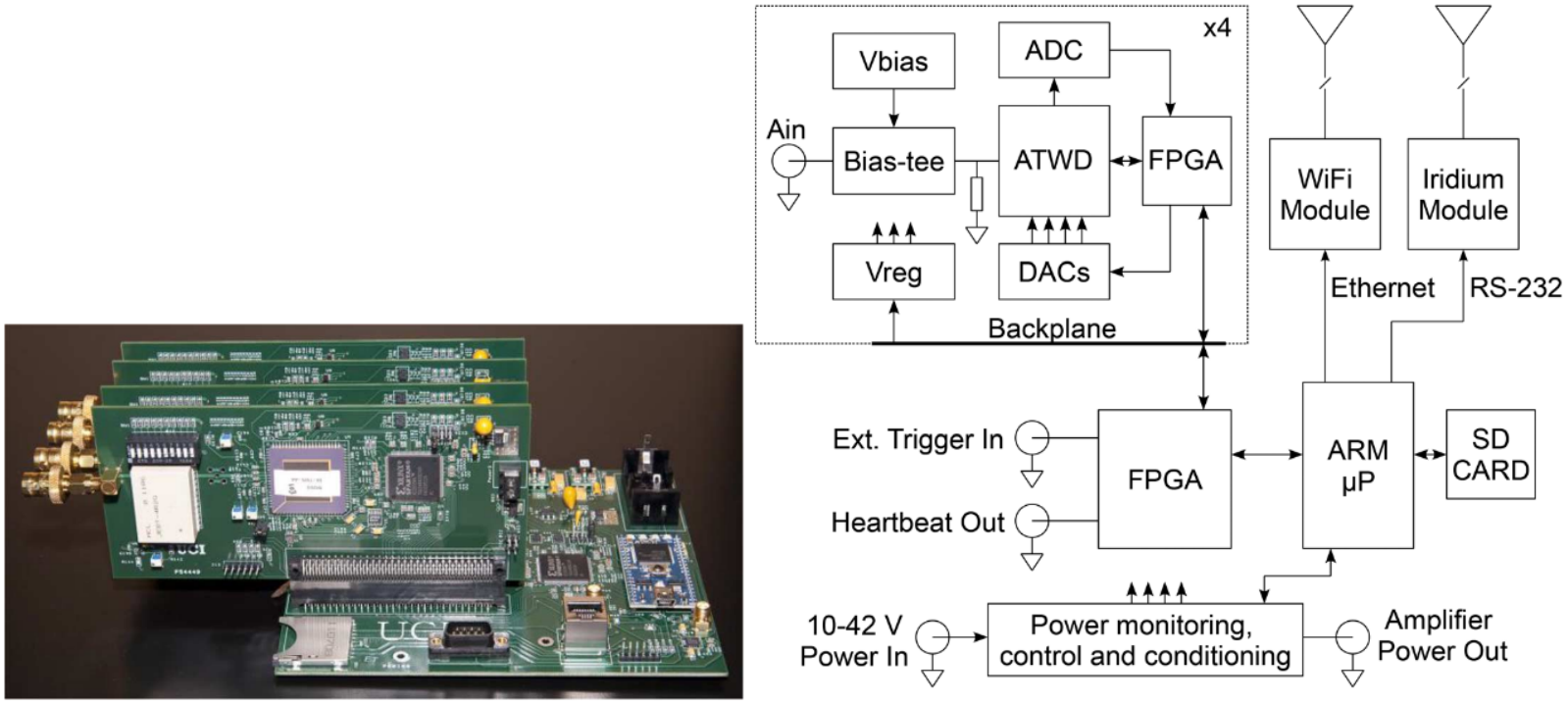

Figure 27: The ARIANNA data acquisition system triggers and digitizes simultaneously the analogue waveforms [6].

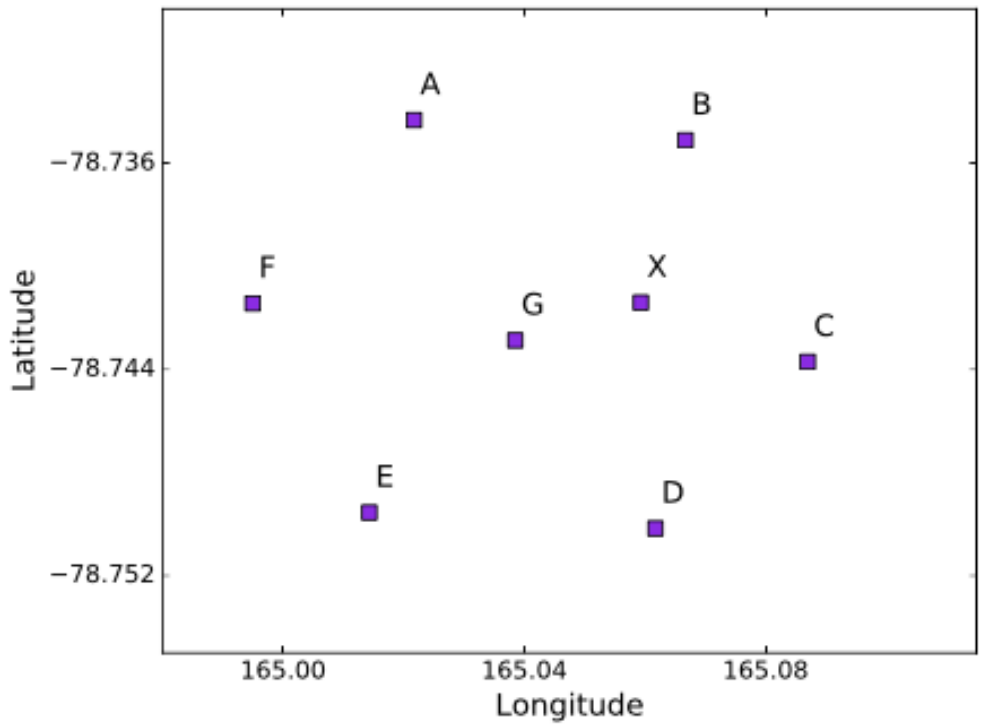

Figure 28: ARIANNA prototype: Hexagonal Radio Array (HRA) [4].

DEPLOYMENT

Figure 29: (Top, left): UCI, crating. (Top, right): UCI shipping. (Bottom, left): Port Hueneme. (Bottom,right): Christchurch, New Zealand

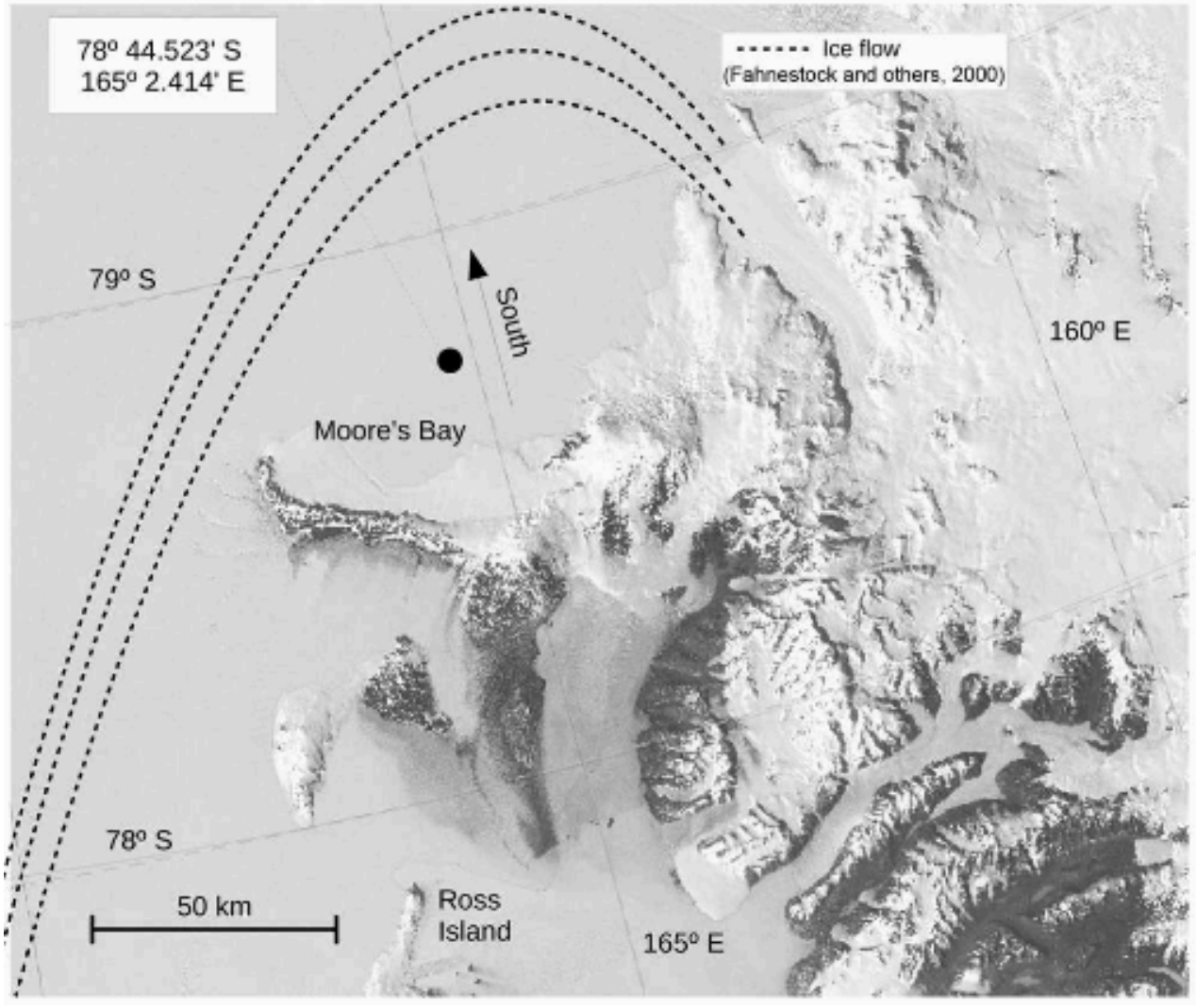

Figure 30: The HRA is located in Moore's Bay [5].

Figure 31: (Top): McMurdo Station, Ross Island. (Bottom): Moore's Bay, Ross Ice Shelf

DEPLOYING ARA2

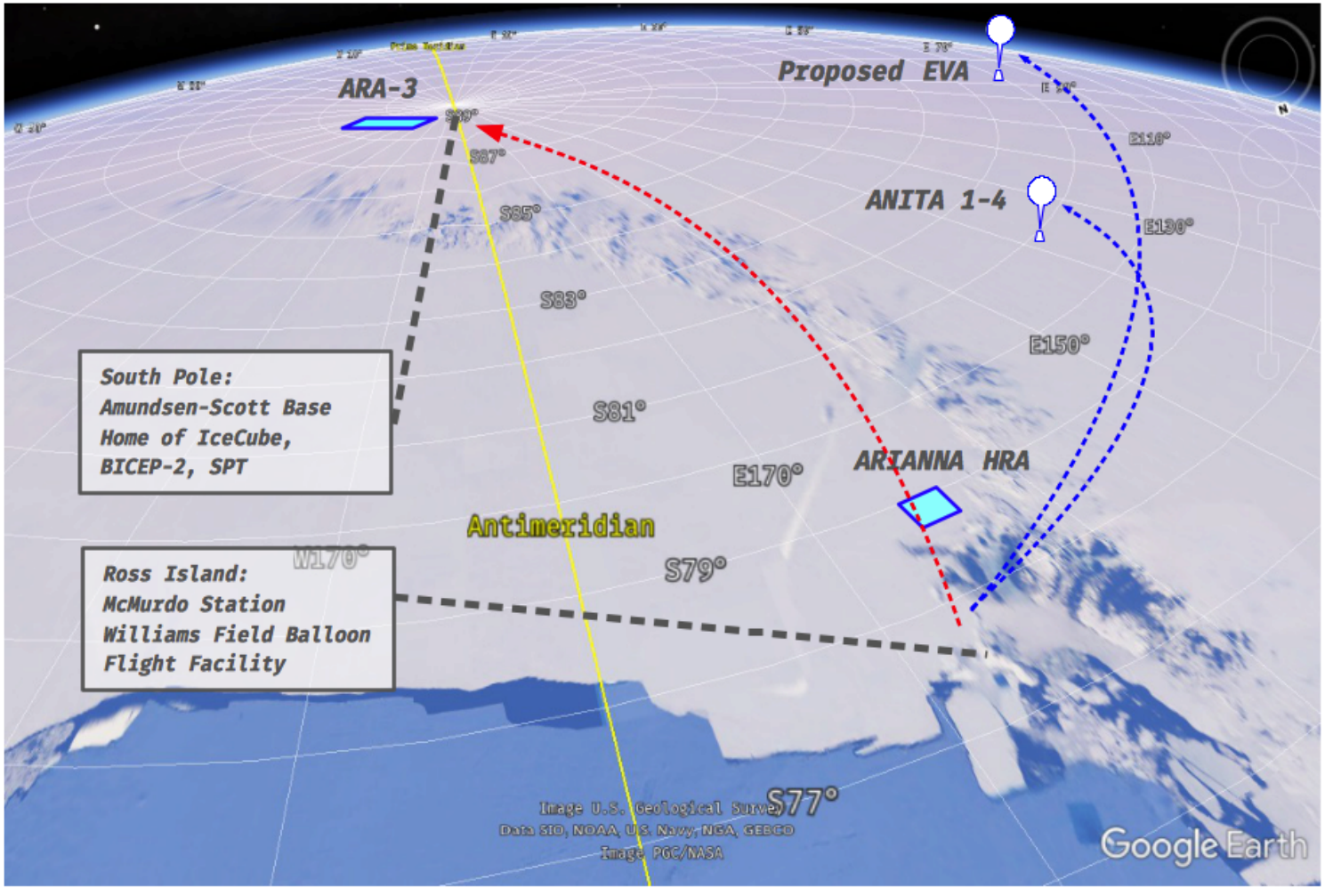

Figure 32: Continuing another 850 miles south to deploy ARA2.

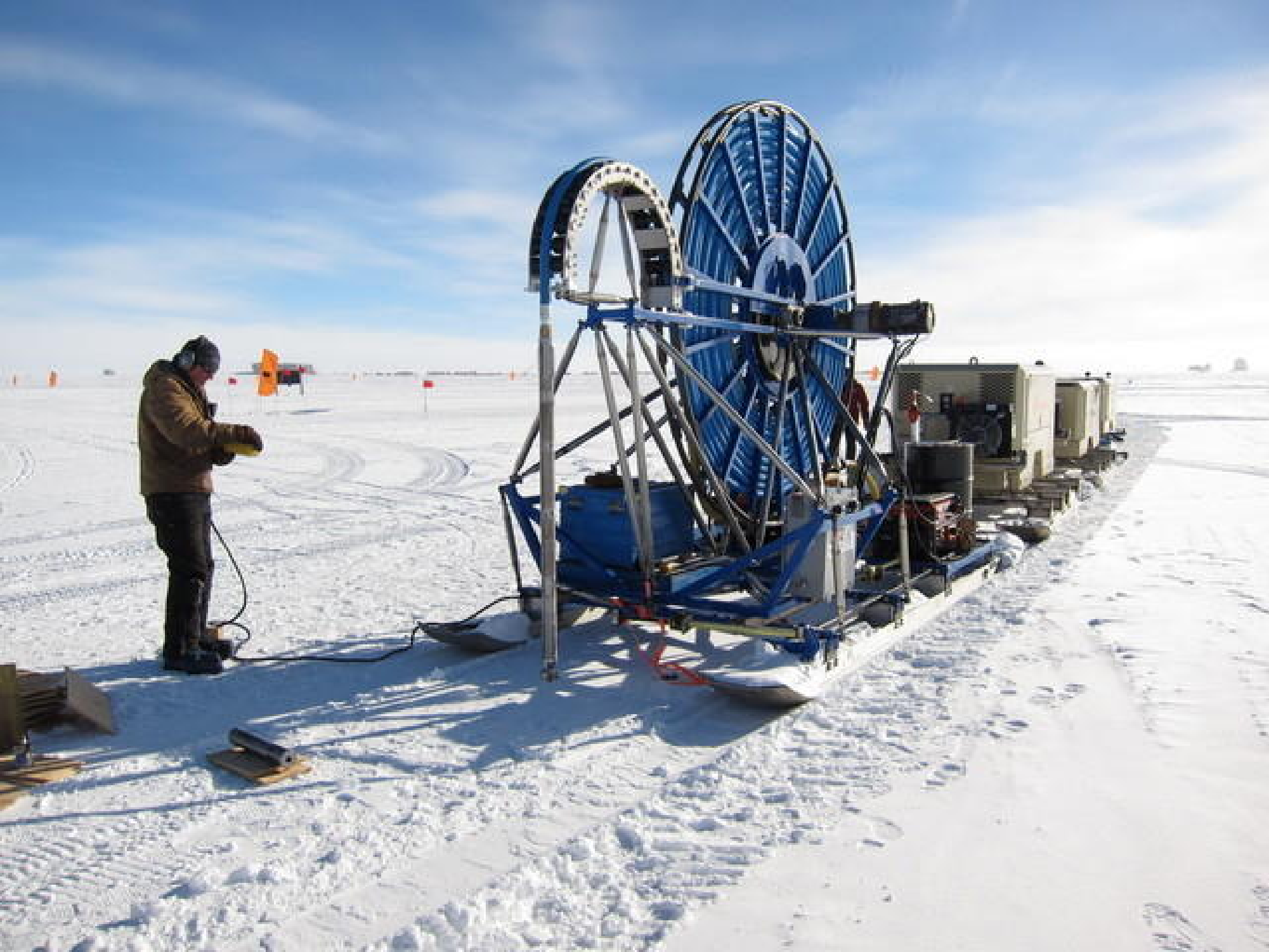

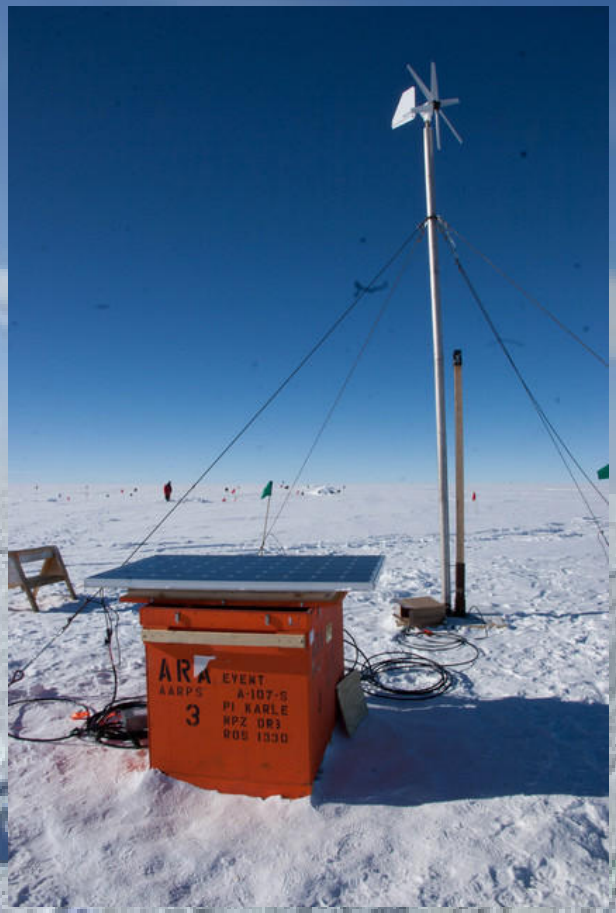
ARA
AARPS
3
EVENT
A-107-S
PI KARLE
NPZ OR3
ROS 1330

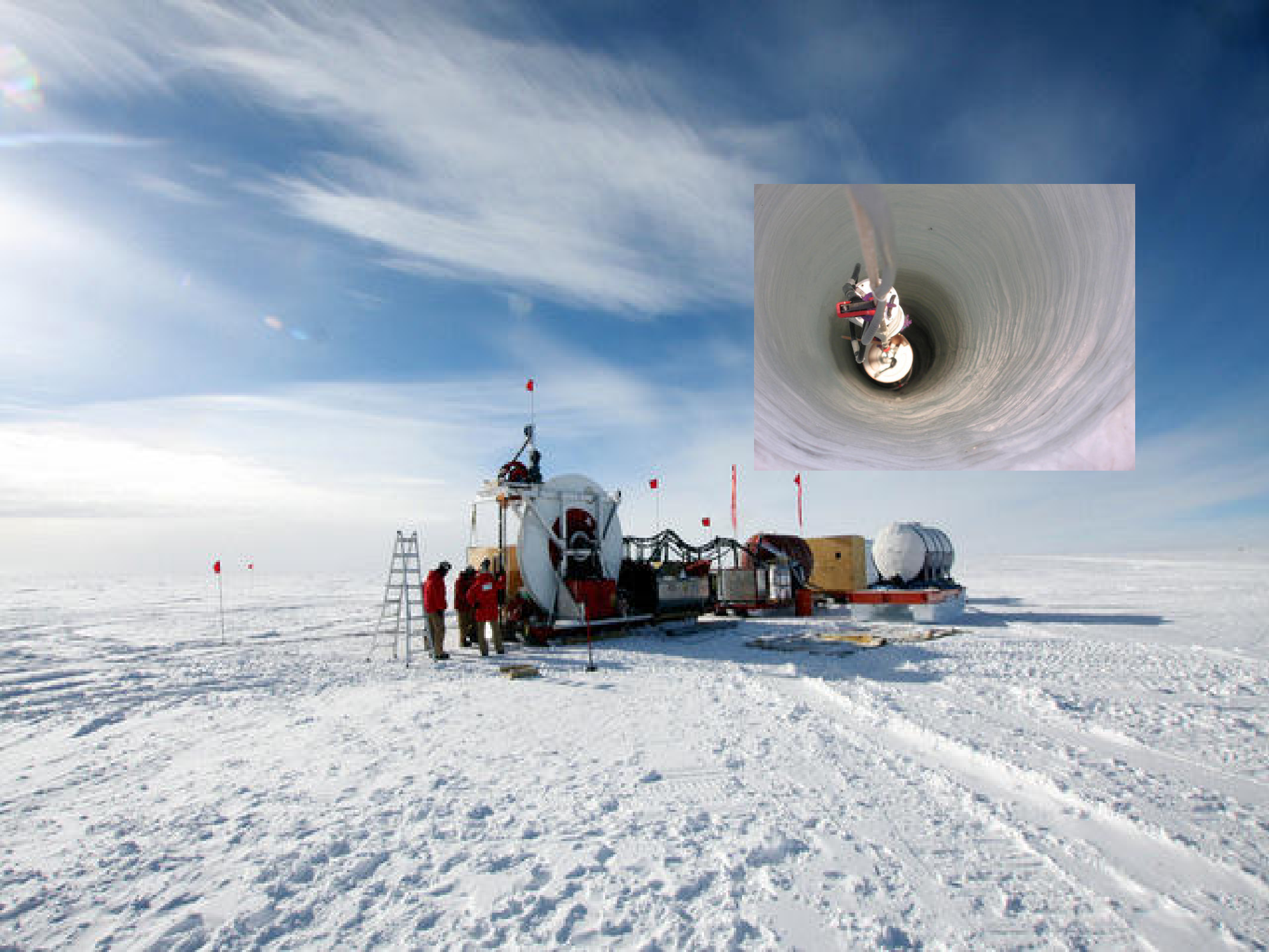

FILM OF ARIANNA DEPLOYMENT - YEAR 2

RESULTS FROM ARA2 AND THE HRA

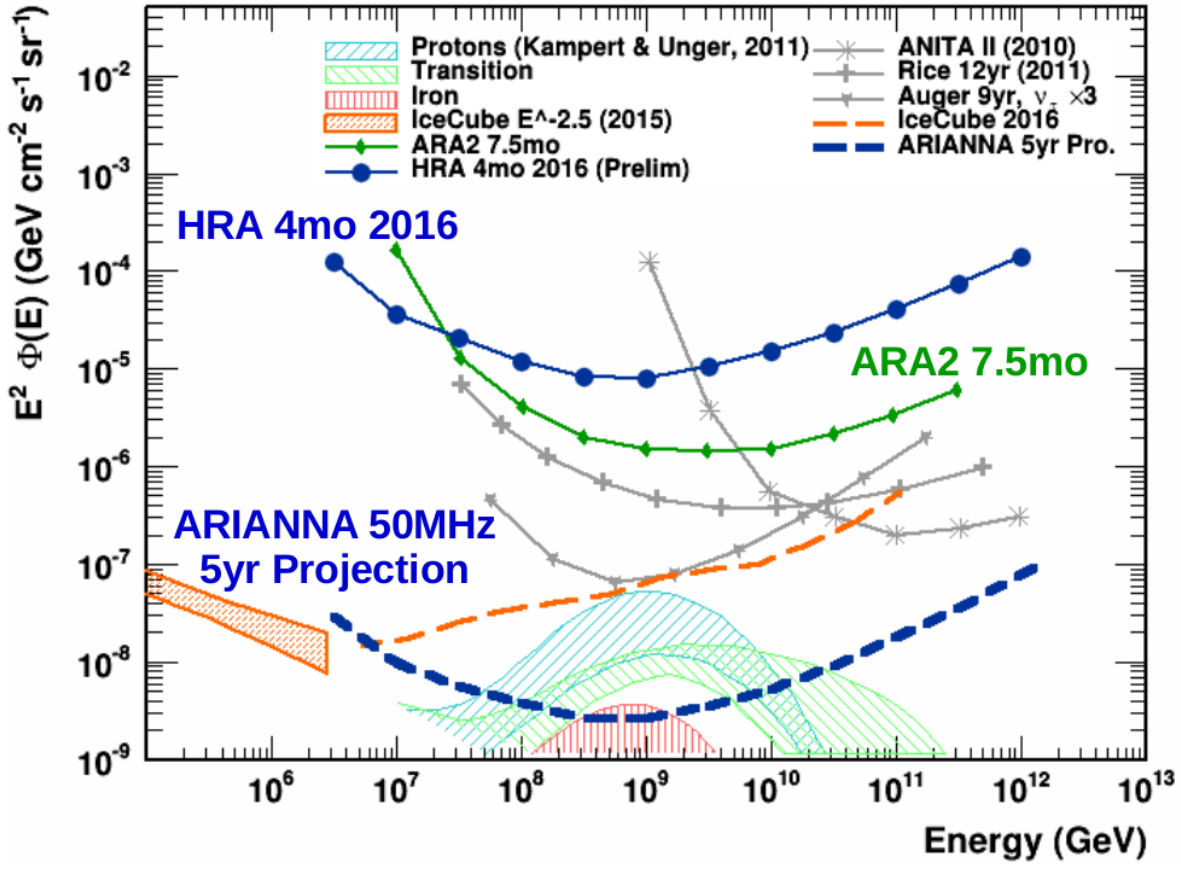

Figure 33: Latest upper-limit on the UHE-ν flux from HRA. Figure courtesy of C. Persichilli, ARA2 Result: [2].

BONUS: HRA DETECTION OF UHECR

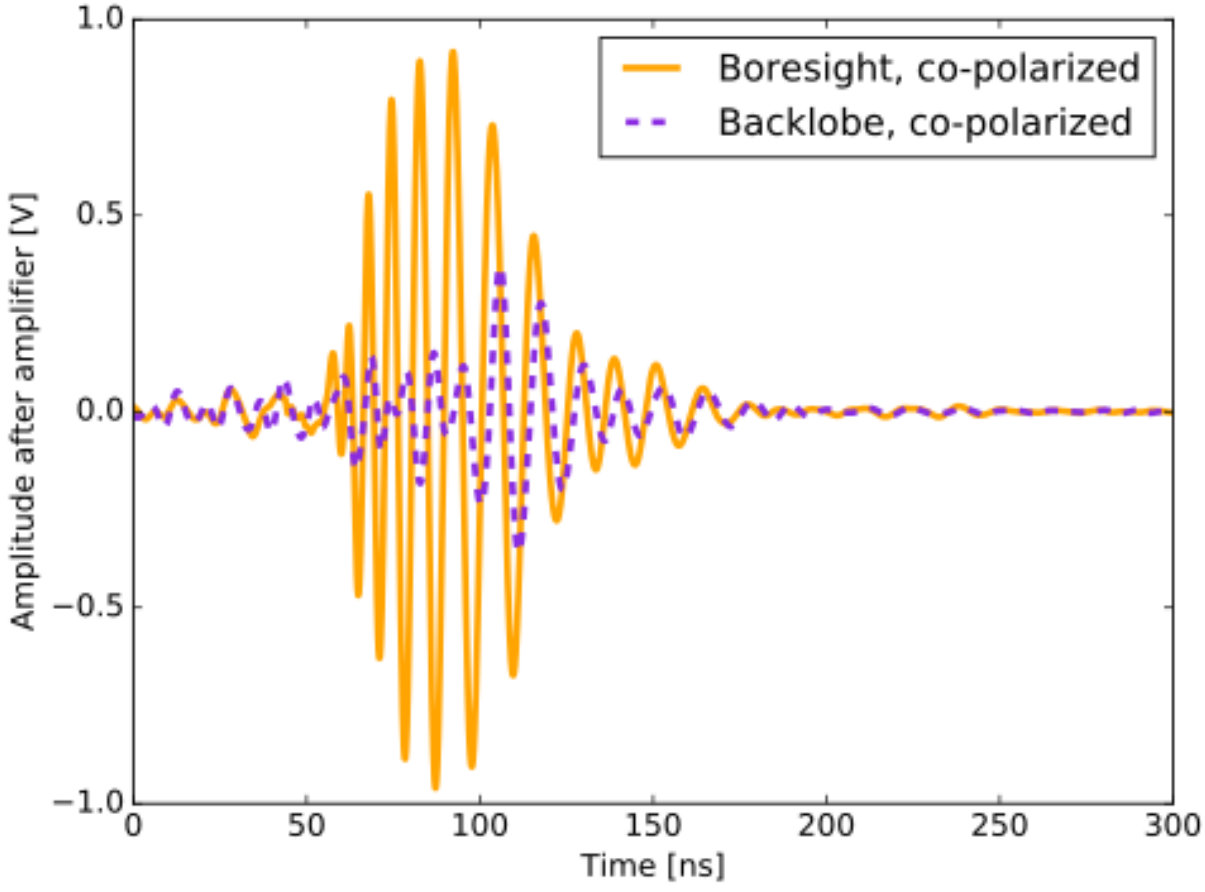

Figure 34: Building a signal template for UHECR [4].

ARIANNA HRA - DETECTION OF UHECR (38 HITS)

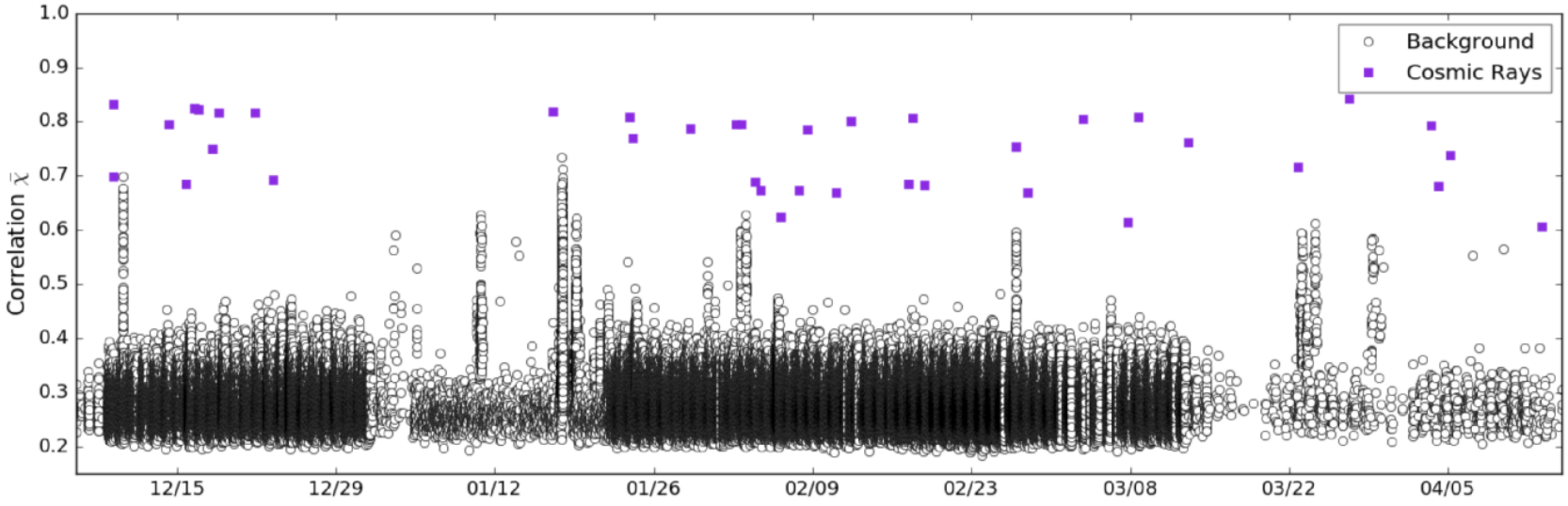

Figure 35: Using signal templates to distinguish signal from backgrounds [4].

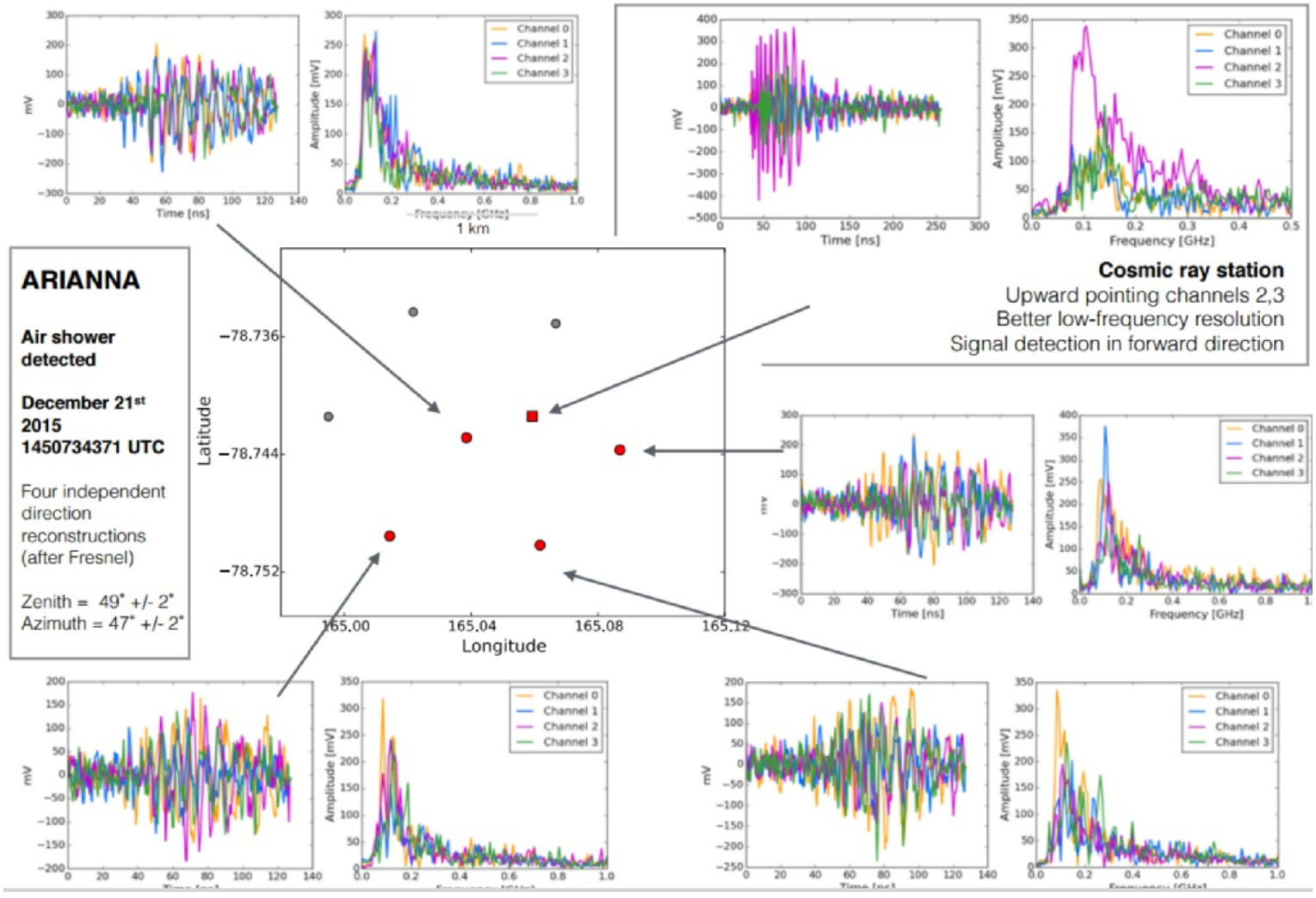

Figure 36: One event hit five stations [4]!

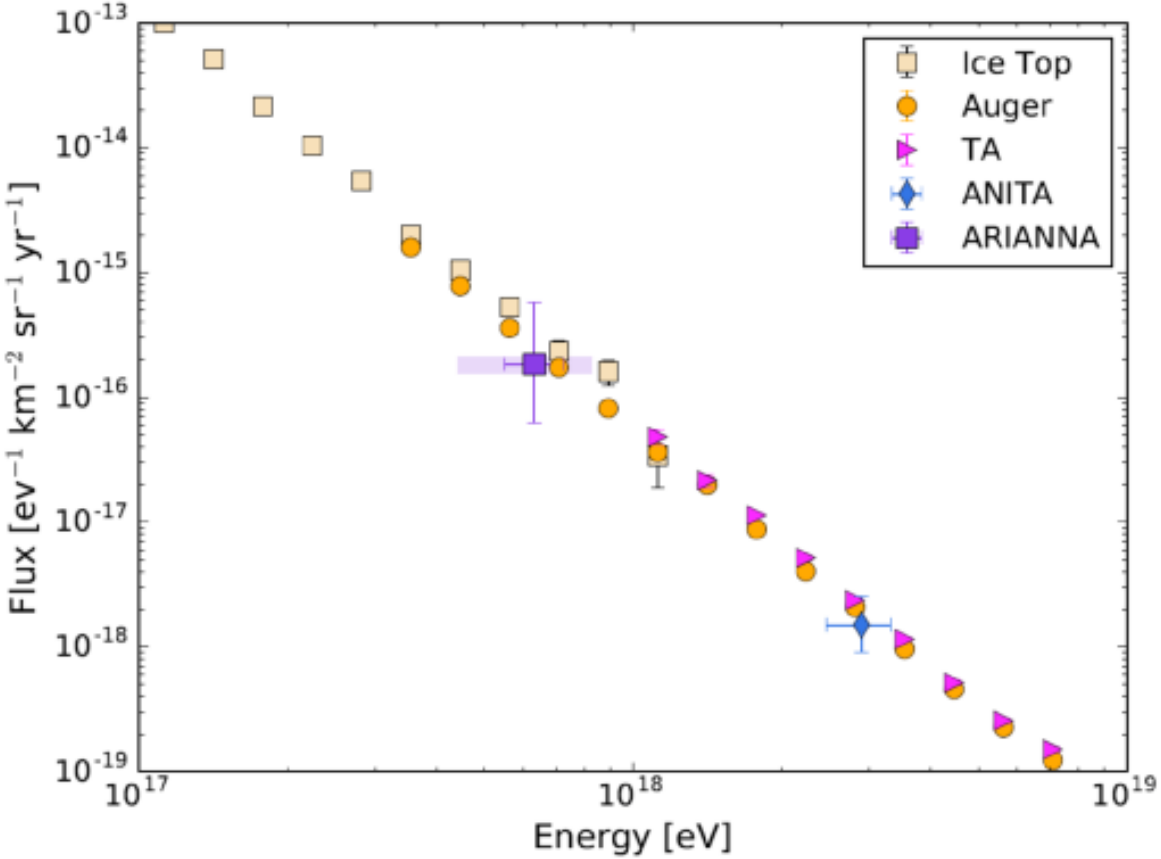

Figure 37: Detection of 38 events leads to a flux measurement, with $\langle E_p \rangle = 0.65^{+1.2}_{-1.0}$ EeV, $J(E) = 1.1^{+1.0}_{-0.7} \times 10^{-16}$ eV^{-1} km^{-2} sr^{-1} [4].

BONUS: ARA DETECTION OF SOLAR FLARES

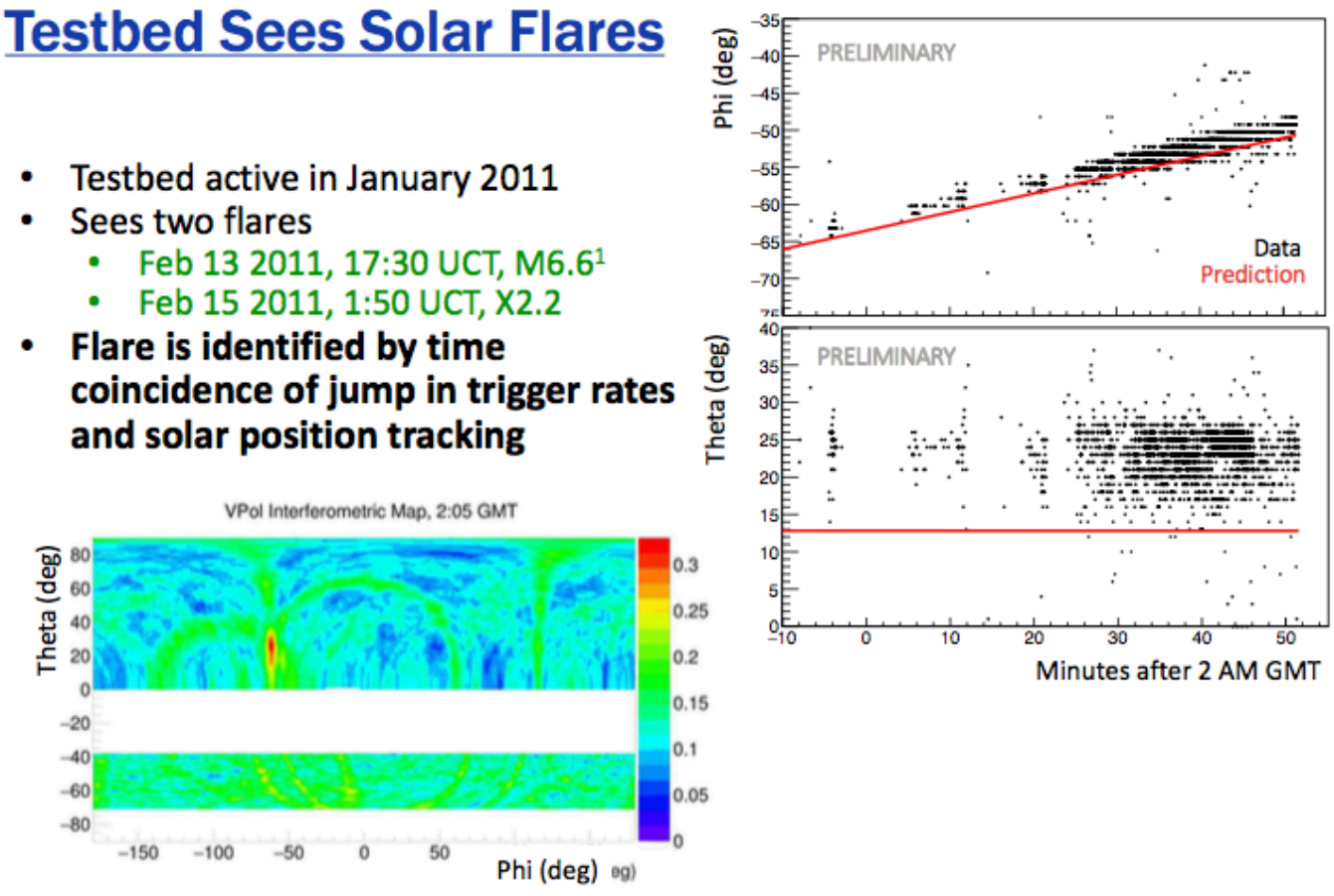

Figure 38: Courtesy of Brian Clark (OSU).

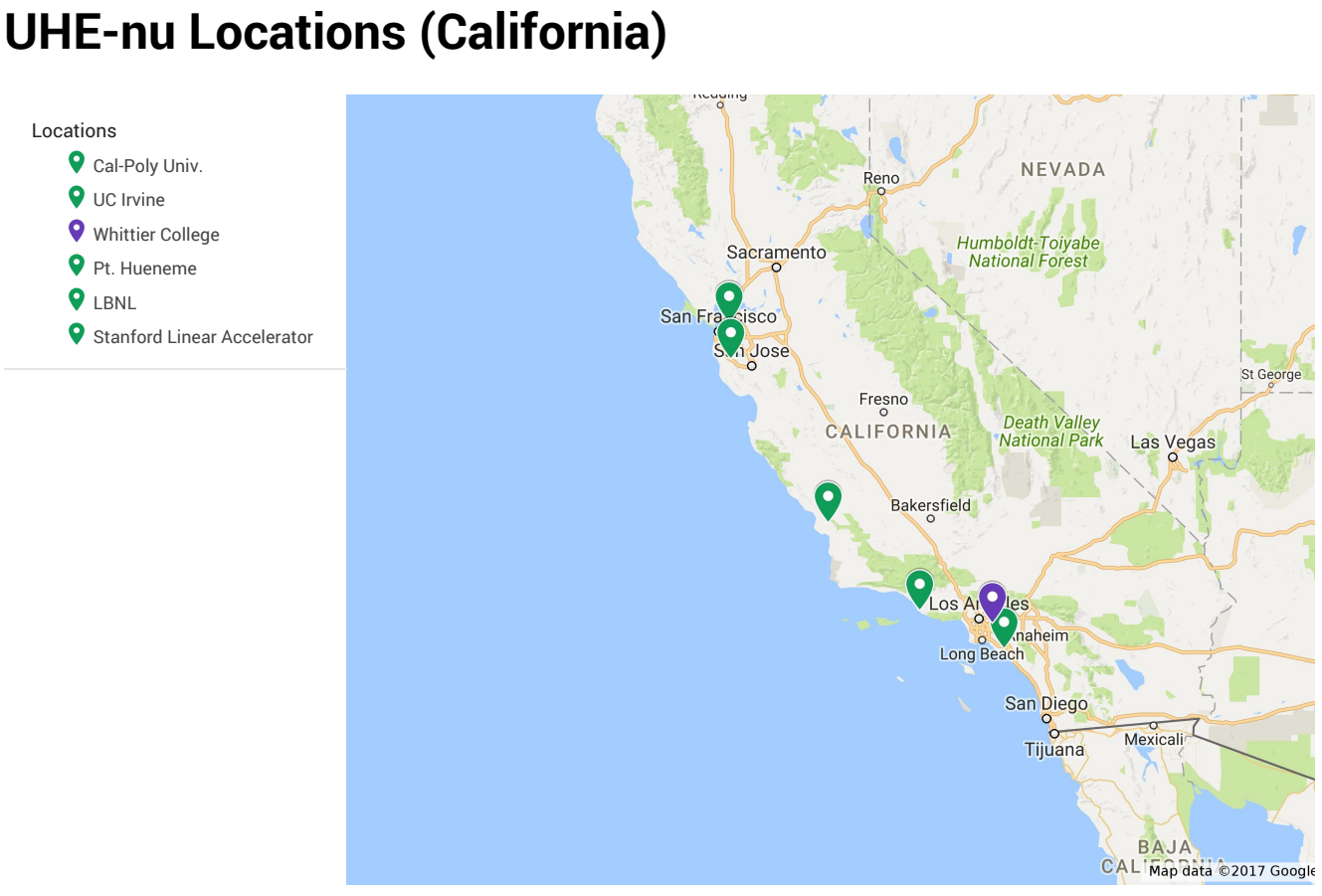

Figure 39: Participating institutions in California.

HUNTING FOR WILD ANTARCTIC ASTRO-PARTICLES

I. **UHE-ν** observations, and a 100-year physics problem
   A. UHE: Ultra-high energy $\approx$ 1 EeV (10^{18} eV), or 0.1 J
II. **Antarctica** is not a *venue*, but a *target*
   A. The Askaryan effect
   B. Ice properties
III. **Undergraduate research with ARA and ARIANNA**
   A. Idea $\rightarrow$ Design $\rightarrow$ Testing $\rightarrow$ Deploy $\rightarrow$ Analysis
   B. Monte Carlo simulations, glaciological modeling
   C. RF circuit/antenna design, systems integration
   D. Logistics
IV. The ARIANNA-HRA, and Recent Results
V. ARA2, and Recent Results
VI. **Future Opportunities**

REFERENCES

[1] A.L. Connolly, A.G. Vieregg. *Neutrino Astronomy - Current Status, Future Prospects*. World Scientific, 2017.

[2] P Allison, R Bard, JJ Beatty, DZ Besson, C Bora, C C Chen, H C Chen, P Chen, A Christenson, A Connolly, J Davies, M Duvernois, B Fox, R Gaior, PW Gorham, K Hanson, J Haugen, B Hill, KD Hoffman, E Hong, Y S Hsu, L Hu, J J Huang, H MA Huang, A Ishihara, A Karle, JL Kelley, D Kennedy, I Kravchenko, T Kuwabara, H Landsman, A Laundrie, J C Li, TC Liu, Y M Lu, L Macchiarulo, K Mase, T Meures, R Meyhandan, C Miki, R Morse, J Nam, RJ Nichol, G Nir, A Novikov, A O'Murchadha, C Pfendner, K Ratzlaff, M Relich, M Richman, L Ritter, B Rotter, P Sandstrom, P Schellin, A Shultz, D Seckel, S Y Shiao, J Stockham, M Stockham, J Touart, GS Varner, Z M Wang, H S Wang, Y Yang, S Yoshida, R Young, and The collaboration. Performance of two askaryan radio array stations and first results in the search for ultrahigh energy neutrinos. *Physical Review D*, 93(8):082003, 2016.

[3] Patrick Allison, Jan Auffenberg, Robert Bard, JJ Beatty, DZ Besson, S Böser, C Chen, Pisin Chen, Amy Connolly, and Jonathan Davies. Design and initial performance of the askaryan radio array prototype EeV neutrino detector at the south pole. *Astroparticle Physics Journal*, 35(7):457–477, 2012.

[4] S W Barwick, D Z Besson, A Burgman, E Chiem, A Hallgren, J C Hanson, S R Klein, S Kleinfelder, A Nelles, C Persichilli, S Phillips, T Prakash, C Reed, S R Shively, J Tatar, E Unger, J Walker, and G Yodh. Radio detection of air showers with the arianna experiment on the ross ice shelf. *arXiv:1612.0447*, 2016.

[5] SW Barwick, EC Berg, D Besson, T Duffin, JC Hanson, SR Klein, SA Kleinfelder, C Reed, M Roumi, T Stezelberger, J Tatar, J Walker, and L Zou. Radar absorption, basal reflection, thickness, and polarization measurements from the ross ice shelf. *Journal of Glaciology*, 2014.

[6] SW Barwick, EC Berg, DZ Besson, T Duffin, JC Hanson, SR Klein, SA Kleinfelder, K Ratzlaff, C Reed, M Roumi, T Stezelberger, J Tatar, J Walker, R Young, and L Zou. Design and performance of the arianna hra-3 neutrino detector systems. *IEEE Transactions on Nuclear Science*, 62(5):2202–2215, 2015.

[7] PW Gorham, SW Barwick, JJ Beatty, DZ Besson, WR Binns, C Chen, P Chen, JM Clem, A Connolly, and PF Dowkontt. Observations of the askaryan effect in ice. *Phys. Rev. Lett.*, 99(17):171101, 2007.

[8] J.C. Hanson and A.L. Connolly. Complex Analysis of Askaryan Radiation: A Fully Analytic Treatment including the LPM effect and Cascade Form Factor. *arXiv:1605.04975*, 2017.

[9] J.J. Beatty, J. Matthews, S.P. Wakely. Particle Data Book, ch. 28. *Particle Data Group*, page 15, 2016.

[10] J.J. Beatty, J. Matthews, S.P. Wakely. Particle Data Book, ch. 28. *Particle Data Group*, page 16, 2016.

[11] P Miočinović, RC Field, PW Gorham, E Guillian, R Milinčić, D Saltzberg, D Walz, and D Williams. Time-domain measurement of broadband coherent cherenkov radiation. *Physical Review D*, 74(4):043002, 6 2006.

[12] M. S. Longair. *High Energy Astrophysics*. Cambridge University Press, 1992.

[13] D Saltzberg, P Gorham, D Walz, C Field, R Iverson, A Odian, G Resch, P Schoessow, and D Williams. Observation of the askaryan effect: coherent microwave cherenkov emission from charge asymmetry in high-energy particle cascades. *Physical review letters*, 86(13):2802–5, 1 2001.

BACKUP SLIDES

UHE-ν RESULTS FROM ARA2

UHE-ν RESULTS FROM ARA2

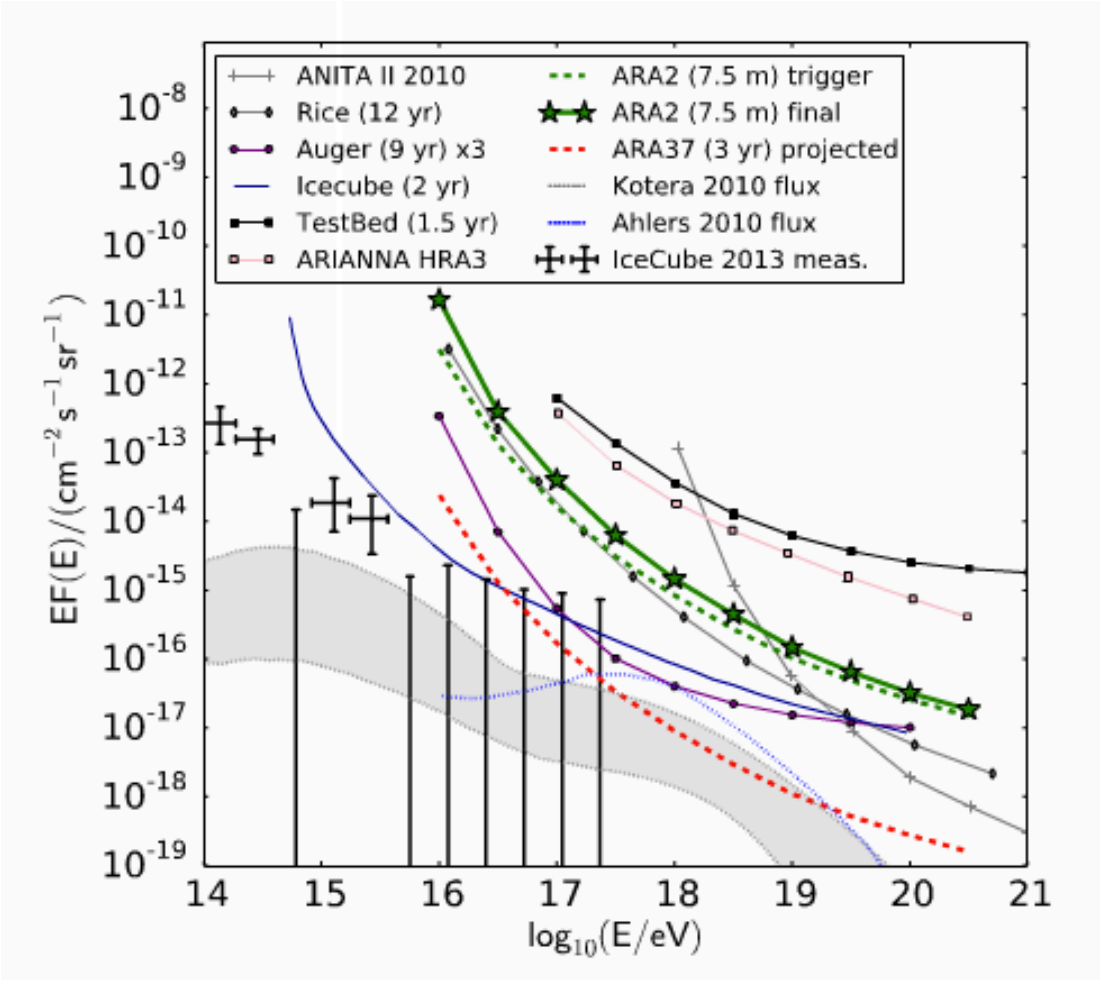

Figure 40: Latest upper-limit on the UHE-ν flux from ARA2 [2].

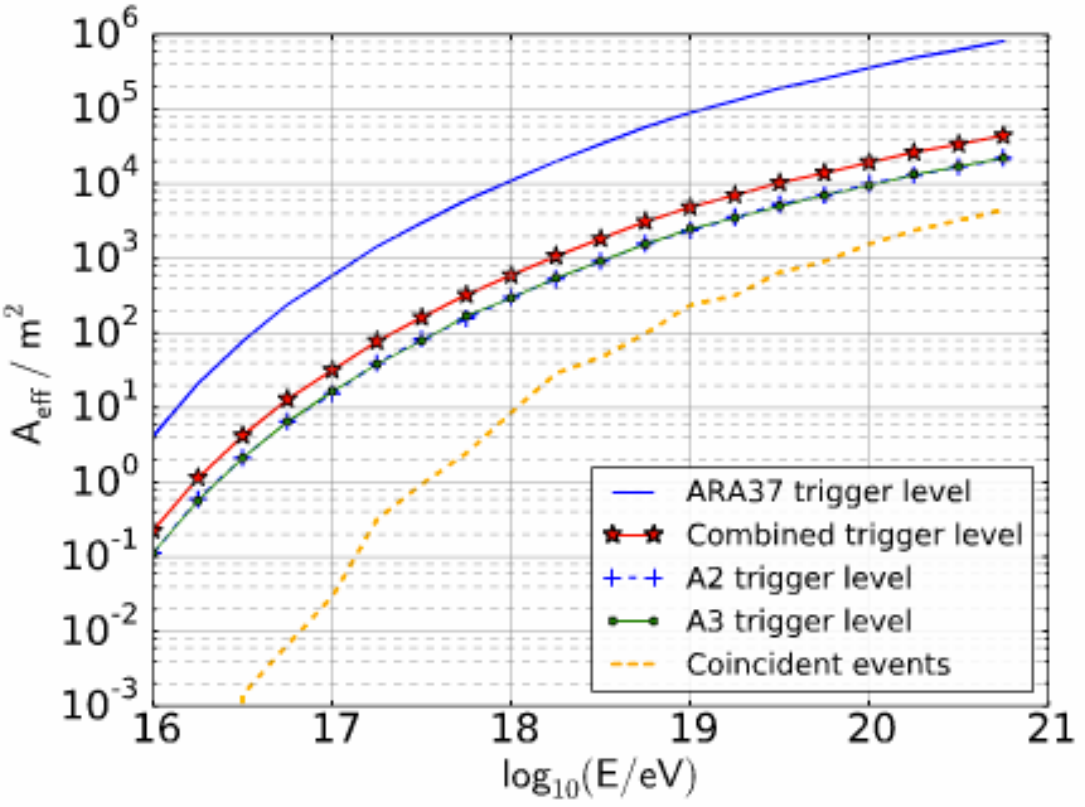

Figure 41: Effective area for the ARA2 limit [2].

UHECR OBSERVATION WITH HRA

Period	Settings
December 6^{th} – January 4^{th}	Trigger 2/2 upward channels, no L1, threshold: 70 mV
January 4^{th} – January 22^{nd}	Trigger 2/2 downward channels, no L1, threshold: 70 mV
January 22^{nd} – February 26^{th}	Trigger 2/2 upward channels, L1 on, threshold: 70 mV
February 26^{th} – March 2^{nd}	Trigger 2/2 upward channels, L1 on, threshold: 72 mV
March 2^{nd} – March 12^{th}	Trigger 2/2 upward channels, L1 on, threshold: 74 mV
March 12^{th} – March 14^{th}	Trigger 2/2 upward channels, L1 on, thresholds: 82 mV
March 12^{th} – April 23^{rd}	Trigger 2/2 upward channels, L1 on, thresholds: 84 mV

Description	Number of events	Fraction	Note
All data	653,447	100%	
After L1	578,745	88%	On station level: 75%
Option 1:			
After cluster cut	538,198	82%	Live-time loss: 6.6%
Events above 150 mV	92	0.01%	Unclear contamination with noise
Option 2:			
Cut on correlation	38	0.005%	$>$ 98% analysis efficiency, 100% live-time

Figure 42: Tables from UHECR observation work [5].

THE ASKARYAN EFFECT

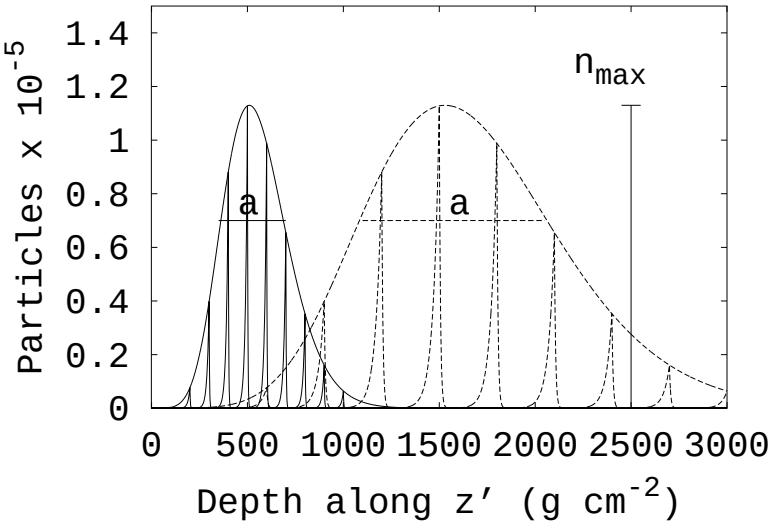

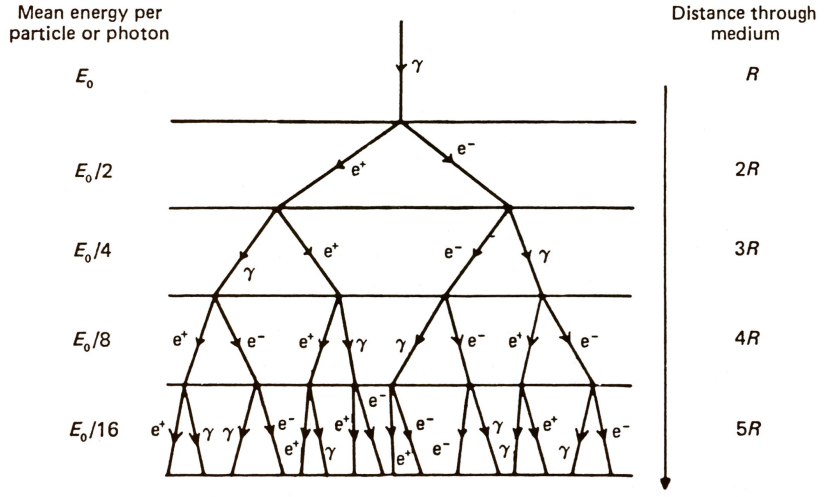

Figure 43: In a UHE cascade, the number of particles increases until the *critical energy* is reached (n_{max}). Medium begins to stop particles after cascade maximum [8] [12].

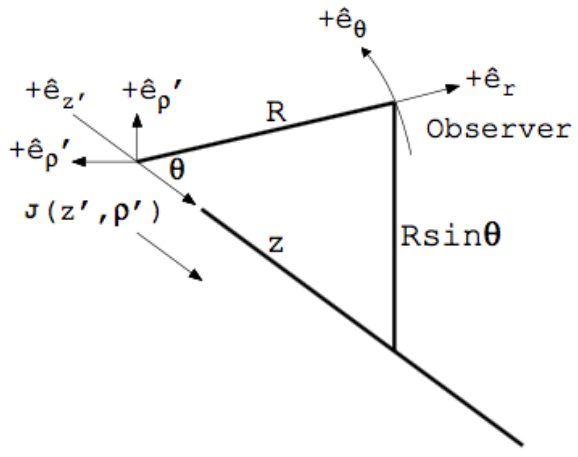

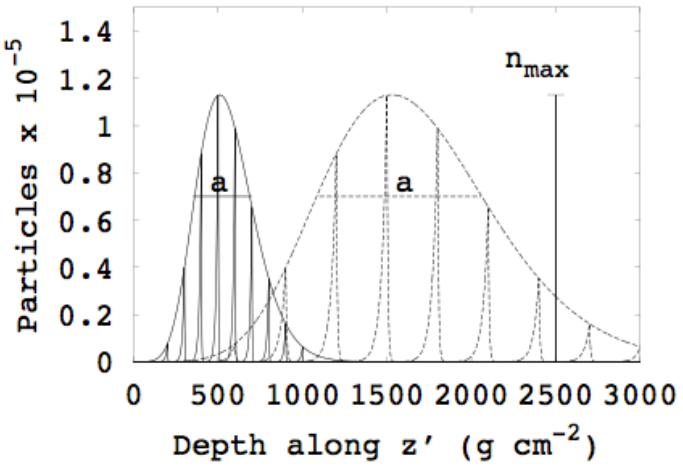

Figure 44: A diagram of the cascade coordinates, and observer coordinates.

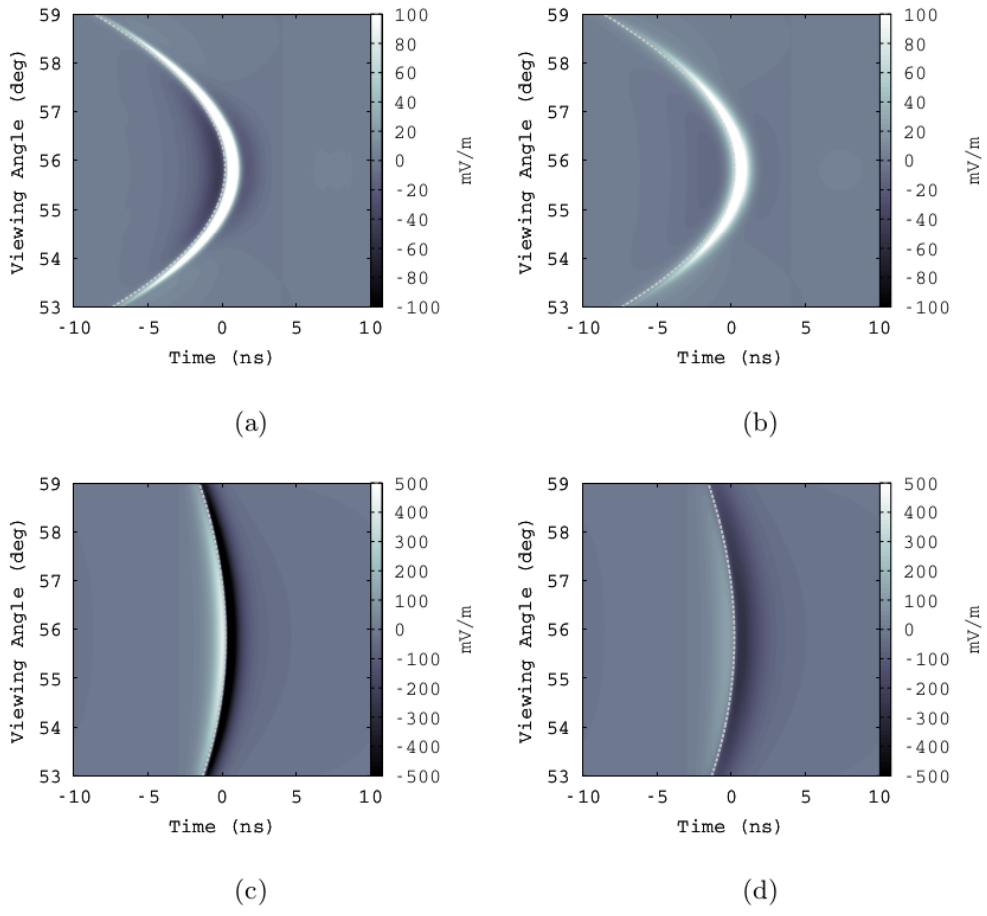

Figure 45: The Askaryan pulse at 1 EeV. (Upper left): $R = 1000$ m, no form factor. (Upper right): $R = 1000$, with form factor. (Lower left): $R = 250$ m, no form factor. (Lower right): $R = 250$ m, with form factor.

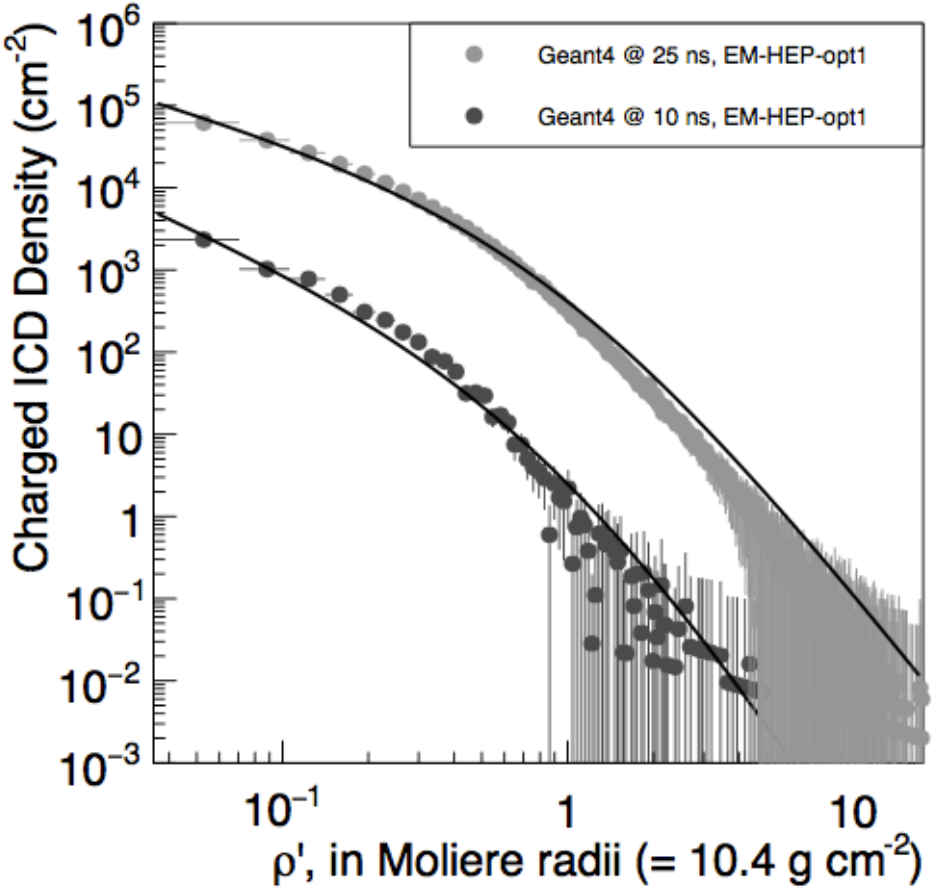

Figure 46: The lateral distribution of charge density for an electromagnetic cascade, at two times after the primary interaction.

GLACIOLOGICAL PARAMETERS

Table 3. Summary of dielectric parameters. The first column is the frequency, ν, followed by the attenuation lengths, which are uncorrected ($\langle L_0 \rangle$) and corrected ($\langle L \rangle$) for $\sqrt{R} = 0.82 \pm 0.07$. The fourth column is $\langle L \rangle$ expressed in dB km^{-1}. The imaginary part of the dielectric constant, ϵ'', is shown in the fifth column. The final column shows $\nu \tan \delta$ (GHz). The typical error on the quantity $\nu \tan \delta$ is 0.2×10^{-4}

ν	$\langle L_0 \rangle$	$\langle L \rangle$	$\langle L \rangle$	$\epsilon'' \times 10^3$	$\nu \tan \delta \times 10^4$
GHz	m	m	dB km^{-1}		GHz
0.100	432	449	19.3	3.8	1.2
0.175	467	487	17.8	2.0	1.1
0.250	457	476	18.2	1.4	1.1
0.325	422	438	19.8	1.2	1.2
0.400	408	423	20.5	1.0	1.3
0.475	366	378	23.0	0.95	1.4
0.550	349	360	24.1	0.86	1.5
0.625	363	375	23.2	0.72	1.4
0.700	331	341	25.5	0.71	1.6
0.775	310	319	27.2	0.69	1.7
0.850	320	329	26.4	0.61	1.6
Ave.	380 ± 16	400 ± 18	22 ± 1	1.3 ± 0.3	1.37 ± 0.06

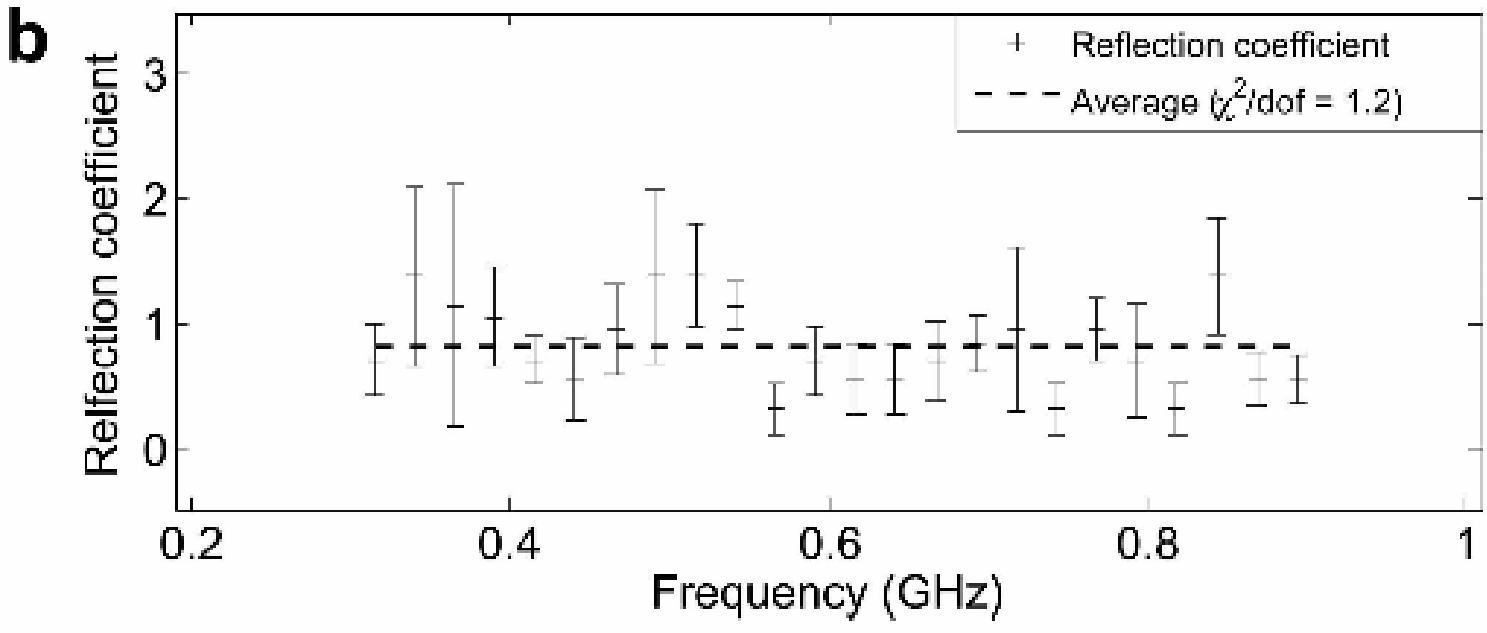

Figure 47: The reflection coefficient in Moore's Bay.